

AXIAL SEGREGATION IN HORIZONTALLY VIBRATED GRANULAR MATERIALS: A NUMERICAL STUDY

by

Ashish Bhateja (Y6105010)



DEPARTMENT OF MECHANICAL ENGINEERING
INDIAN INSTITUTE OF TECHNOLOGY KANPUR

June, 2008

AXIAL SEGREGATION IN HORIZONTALLY VIBRATED GRANULAR MATERIALS: A NUMERICAL STUDY

A Thesis submitted

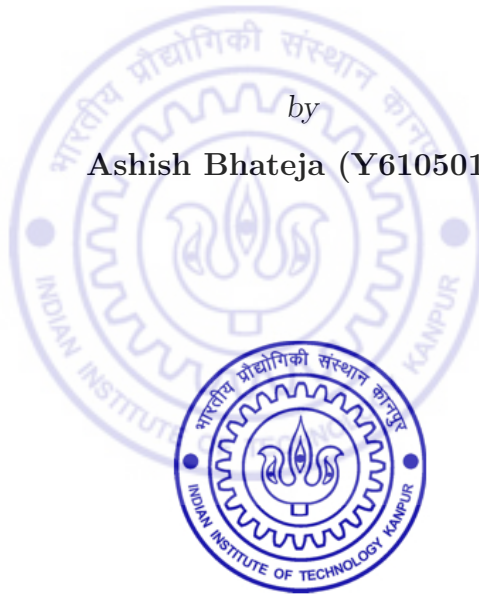
in partial fulfillment of the requirements

for the Degree of

Master of Technology

by

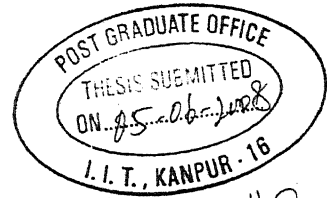
Ashish Bhateja (Y6105010)



to the

**DEPARTMENT OF MECHANICAL ENGINEERING
INDIAN INSTITUTE OF TECHNOLOGY KANPUR**

June, 2008



ii

CERTIFICATE

It is certified that the work contained in the thesis entitled "*Axial segregation in horizontally vibrated granular materials: A numerical study*" has been carried out by *Ashish Bhateja* under my supervision and that this work has not been submitted elsewhere for a degree.

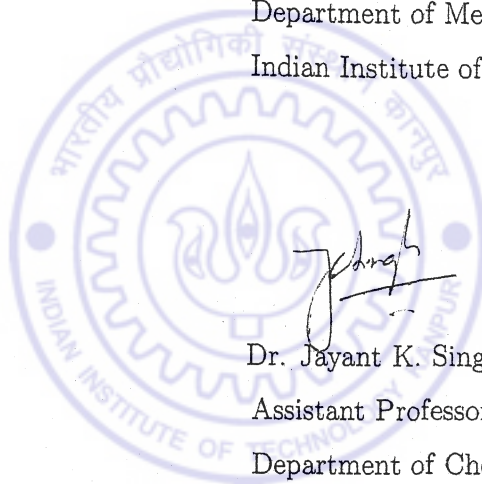
Dr. Ishan Sharma

Assistant Professor

Department of Mechanical Engineering

Indian Institute of Technology Kanpur

June, 2008



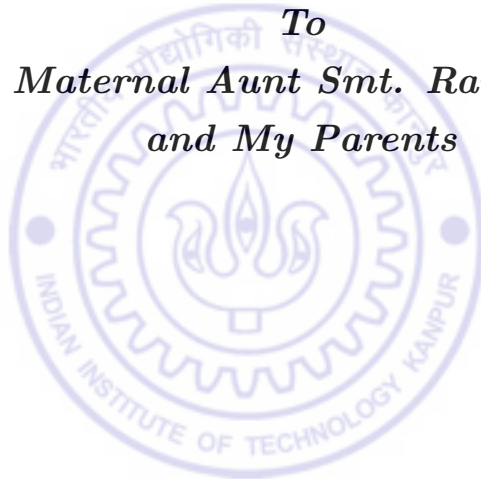
Dr. Jayant K. Singh

Assistant Professor

Department of Chemical Engineering

Indian Institute of Technology Kanpur

Dedicated
To
My Maternal Aunt Smt. Ranju Arora
and My Parents



Acknowledgements

It gives me immense pleasure to gratitude my thesis supervisors Dr. Ishan Sharma and Dr. Jayant K. Singh for giving me an opportunity to carry out this project work. Their systematic approach to all matters has been a significant influence on my way of working. The freedom provided by them made me take risks and do new experiments which turned out to be fruitful consequently. I am highly indebted to Dr. Jayant K. Singh for providing a friendly atmosphere in the lab which made my work easier.

I also pay my special thanks to Dr. Anindya Chatterjee and Dr. Pankaj Wahi for their suggestions. The discussion with them always turned out to be a turning point in my thesis work.

I would like to thank my Lab mates Satyapal Singh, Sudhir, Naresh, Ashim, Kumar, Anitya, Subimal, Viswa, Sandip for their cooperation and support in hard times of my research work. I enjoyed with them and the same time learned a great deal from them. The time spent with them will be a sweet memory for me forever my life.

I am also thankful to my friends Sumeet, Vikulp, Lavanjay, Amit, Venu and Subhash for giving me the support when needed. The time spent with them is unforgettable. I also want to thank Neeraj Kathuria, my spiritual and philosophical friend, interaction and sharing with whom was always fun.

Finally, I thank my maternal aunt Smt. Ranju Arora and my parents for supporting me throughout my life and having faith in me. I would not have reached here without their support, guidance and love.

Ashish Bhateja

Department of Mechanical Engineering

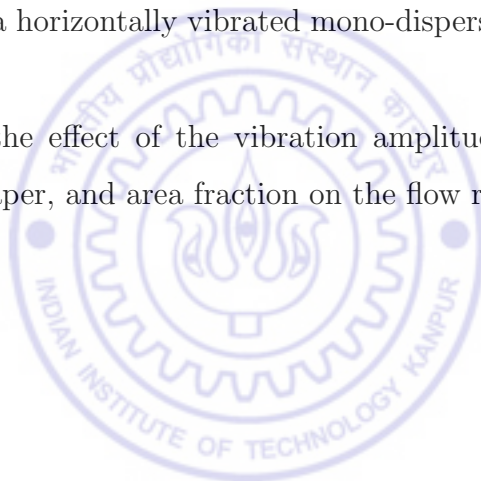
Indian Institute of Technology Kanpur

June 2008

Abstract

It is known that a horizontally vibrated binary mixture in a tapered and inclined channel segregates axially, with each of the two species moving to the opposite ends of the channel. In general, the parameters that affect the segregation process include the vibration frequency and its amplitude, the constituents' mass, size and their material properties, and the channel's taper and inclination. The ultimate goal is to locate those parameters that are most significant to the segregation process, thereby providing control variables for practical applications. However, owing to the complexity of the problem, as a first step to better understand the physics behind this phenomenon, we undertake three dimensional discrete-element simulations of a horizontally vibrated mono-disperse granular particles in a tapered and inclined channel.

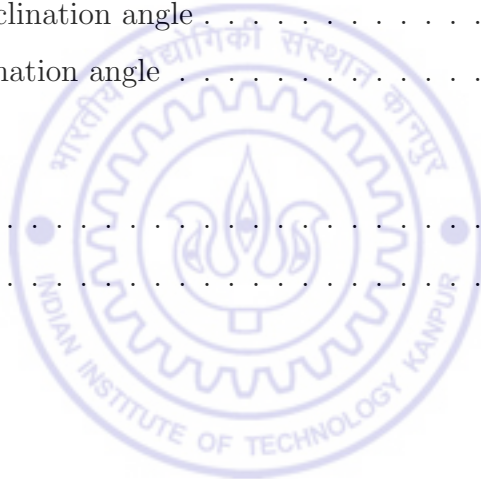
We have investigated the effect of the vibration amplitude and frequency, the channel's inclination angle and taper, and area fraction on the flow rates of granular particles.



Contents

1	Introduction	1
1.1	Problem statement	2
1.2	Overview	2
2	Literature review	5
3	Simulation methodology	12
3.1	Molecular Dynamics simulation	12
3.2	Monte Carlo simulation	14
3.3	Discrete element method	15
3.4	Force laws	16
3.4.1	Normal force	17
3.4.2	Tangential force	22
3.5	Integration algorithm.	24
3.5.1	Verlet algorithm	25
3.5.2	Leapfrog algorithm	27
3.5.3	Velocity Verlet algorithm	27
3.6	Our simulation algorithm	28
4	Validation tests for DEM code	31
4.1	Acceleration of a particle rolling down an inclined plane	32
4.2	Particle-particle or particle-wall forces	32

4.2.1	Zero damping	33
4.2.2	Finite damping	33
4.3	Vibrating channel with parallel side walls and zero inclination	36
4.4	Vibrating channel with parallel side walls and inclination	37
5	Results and discussion	41
5.1	Amplitude variation	43
5.2	Theta variation	45
5.3	Area fraction variation	46
5.4	Variation in the channel's taper	50
5.4.1	Zero inclination angle	50
5.4.2	1° inclination angle	53
6	Conclusions	56
6.1	Conclusion	56
6.2	Future work	57
	Bibliography	58



List of Figures

1.1	Top view of an actual vibrating channel	3
1.2	Three-dimensional view of the vibrating channel	3
1.3	Top and side view of the vibrating channel	4
2.1	Brazil-nut effect: Large ball rising to the top	6
2.2	(a). Initial position of large glass bead (b). Configuration after few taps (c). Large glass bead reaches top after several taps, Knight et al. (1993)	7
2.3	(a). Configuration of the glass beads after several taps. Black glass beads on the right side of the container reaches bottom due to the roughness of the right wall while the beads in contact with the left smooth wall doesn't get affected. (b). Positions of glass beads in a conical shaped container after several taps, Knight et al. (1993)	8
2.4	Horizontal Segregation in a vertically vibrated granular bed for different den- sity ratios, Duncan et al. (2004)	9
2.5	Large particles segregates horizontally in vertically vibrated granular system, Levanon & Rapaport (2001)	10
2.6	Axial segregation of grains in a rotating cylinder, Rapaport (2002)	10
3.1	An algorithm of molecular dynamics simulation	13
3.2	Contact between two particles	16
3.3	Schematic of force model	18
3.4	Lennard-Jones Potential with the distance between particles	19

3.5	Variation of Lennard-Jones force with the distance between particles	20
3.6	Coulomb friction model: A limiting friction force to prevent sliding occur between particles	23
3.7	Particle interaction with system's boundary wall	24
3.8	Schematic of Verlet algorithm in simulation	26
3.9	Schematic of Leapfrog algorithm in a simulation	28
3.10	Schematic of Velocity Verlet algorithm in a simulation	29
3.11	Three-dimensional view of particles arranged on top of the channel	30
3.12	Top view of configuration of particles after dropping into the channel	30
4.1	Sphere rolling down an inclined channel (a) No damping in the system (b) System with finite damping	32
4.2	Height of particle from the surface vs time. Height is in multiples of particle diameter and time is non-dimensionalized so that one unit of simulation time approximately equals to 0.018 s.	33
4.3	Normal elastic force on a particle by channel's base vs time. Normal force is also non-dimensionalized by the particle's mass, and the acceleration due to gravity.	34
4.4	Height of particle from the channel's base vs time. Particle come to rest after collisions with the channel's base in infinite time.	35
4.5	Normal elastic force on a particle by the channel's base vs time.	35
4.6	Normal damping force vs time	36
4.7	Top and side view of a vibrating channel with parallel side walls and zero inclination	37
4.8	Fractional and net flow rate of particles in a vibrating channel with parallel side walls and zero inclination	38
4.9	Top and side view of a vibrating channel with parallel side walls and inclination θ	39

4.10	Density distribution of particles from simulation transverse to the direction of vibration	40
4.11	Density distribution of particles from experiment transverse to the direction of vibration	40
4.12	Density distribution of particles from simulation along the direction of vibration	40
4.13	Density distribution of particles from experiment along the direction of vibration	40
5.1	Top view of vibrating channel	42
5.2	Effect of vibration amplitude on the downward flow rate of grains	43
5.3	Effect of vibration amplitude on the upward flow rate	44
5.4	Effect of vibration amplitude on the net flow rate.	45
5.5	Effect of inclination on the grains' downward flow rate.	46
5.6	Effect of inclination on the upward flow rate.	47
5.7	Effect of inclination on the net flow rate.	47
5.8	Effect of area fraction on the grains' downward flow rate	48
5.9	Effect of area fraction on the upward flow rate	49
5.10	Effect of area fraction on the net flow rate	50
5.11	Effect of varying the channel's taper on downward flow rate at zero inclination angle.	51
5.12	Effect of varying the channel's taper on upward flow rate at zero inclination angle.	52
5.13	Effect of varying the channel's taper on net flow rate at zero inclination angle	53
5.14	Effect of the taper on the downward flow rate in a channel inclined at 1° . . .	53
5.15	Effect of the taper on the upward flow rate in a channel inclined at 1°	54
5.16	Effect of the taper on the net flow rate in a channel inclined at 1°	55

Chapter 1

Introduction

Granular materials are ubiquitous. In everyday life, we come across many things that count as granular substances, like wheat, corn flakes, rice, coal etc. There are many natural and industrial phenomenon that involves granular particles. Example of natural phenomenon includes snow avalanches, sand dunes, and landslides. Industrial processes involving handling of grains are hopper flows, milling, grinding, fluidized beds, segregation etc. The interaction between the grains is highly dissipative due to inelastic collisions and friction. Therefore, kinetic energy is not conserved in a granular system, and an external source of energy in some form must be applied to sustain the motion of a system of granular particles.

These materials possess peculiar properties that are not displayed by conventional substances. Granular materials can behave like solids, liquids or gases depending upon applied external conditions (Jaeger and Nagel 1996). Apart from these properties, there are many other phenomena unique to these substances. It is observed that granular mixtures tend to segregate into their constituent species, when shaken externally. A common example is the ‘Brazil-nut effect’ (Rosato et al. 1987) in which a large particle, mixed with the smaller particles, separates to the top when vibrated vertically. However, under different conditions this big particle can sink to the bottom of the vertically shaking container, thereby demonstrating the ‘Reverse Brazil-nut effect’ (Shinbrot and Muzzio 1998). It is not always the case that particles segregate only in the shaking direction, horizontal segregation of grains

can also occur. There are systems, in which particles segregate in a direction transverse to the shaking direction (Levanon and Rapaport 2001). This is also a feature of our system. Because segregation plays a very important role in industry, particularly pharmaceutical and agricultural industries, significant efforts have been invested into understanding this phenomenon.

1.1 Problem statement

It is observed in the industry that a granular mixture segregates axially in a horizontally vibrated channel, which is slightly inclined to the ground. This channel has a zigzag internal profile as shown in Fig. 1.1. Typically, a mixture of grains such as wheat (heavy) and chaff (light) is poured into the center of the channel, as shown in Fig. 1.1, which, as shown, is shaken in a direction perpendicular to the channel's axis. It is observed that the heavy and light grains move towards the lower (A) and higher (B) ends, respectively. The separation achieved is nearly faultless.

We begin by first conjecturing that the channel's Christmas tree pattern is really a concatenation of small trapezoidal chambers as shown in Fig. 1.1, with each chamber acting as a micro-sorter. The sorting itself is hypothesized to be a result of the competition between gravity, which pulls material down towards the lower narrow end of the trapezium, and the collisional momentum transfer from the tapered walls that is biased upwards. To completely understand the granular dynamics in whole segregating channel, we first concentrate our study on one micro-sorting vibrating channel, as shown in Figs. 1.2 and 1.3.

1.2 Overview

A literature review of work related to segregation of granular materials is presented in Chapter 2. In Chapter 3, various simulation methodologies are described, and a detailed discussion on these techniques along with several force laws is presented. We validate our code in Chap-

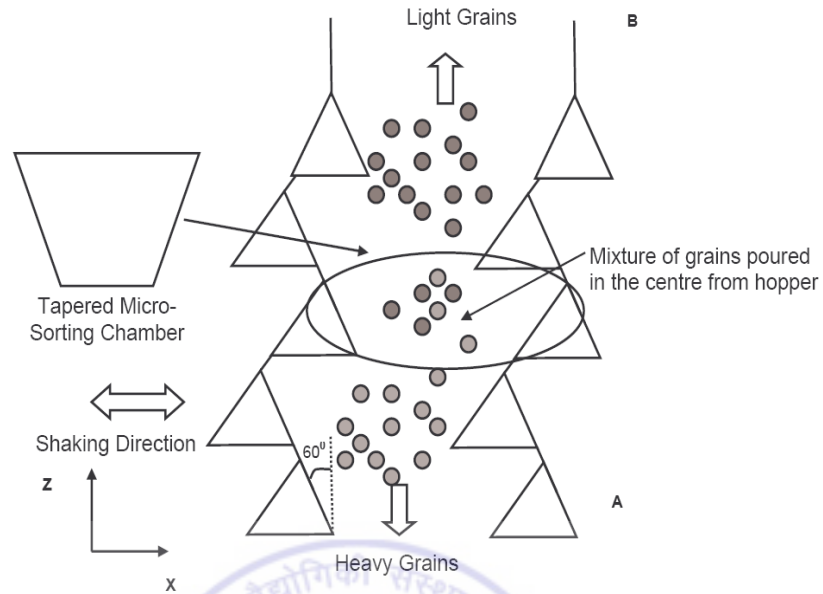


Figure 1.1: Top view of an actual vibrating channel

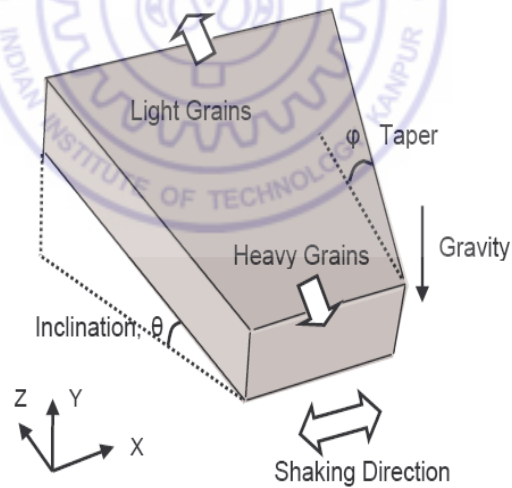


Figure 1.2: Three-dimensional view of the vibrating channel

ter 4. Finally, in Chapter 5, some results are discussed. We conclude our work in Chapter 6, along with some thoughts for the future.

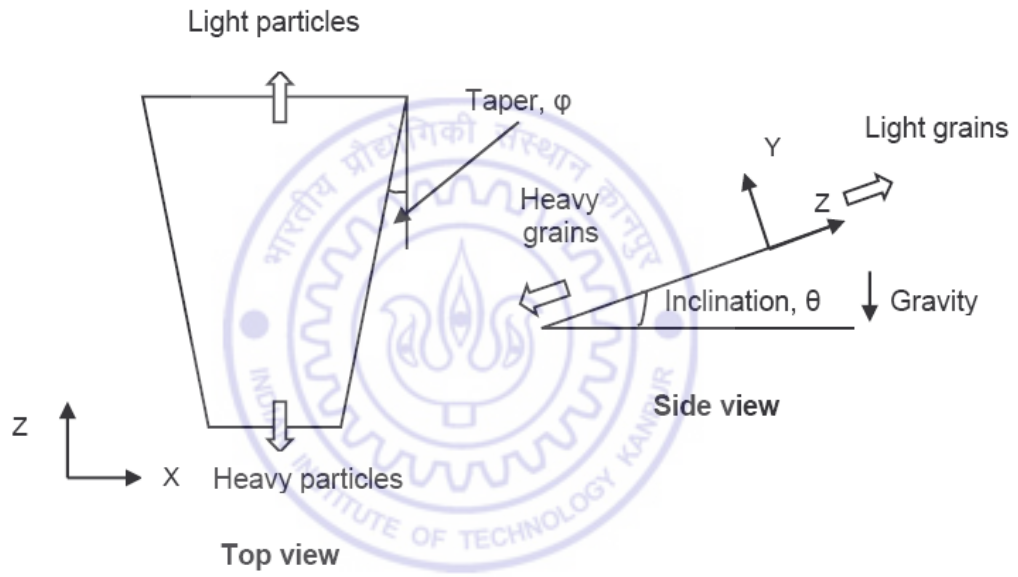


Figure 1.3: Top and side view of the vibrating channel

Chapter 2

Literature review

A review of previous work related to segregation of granular materials is presented in this chapter.

Many experimental and numerical studies have been performed to explore the various parameters that cause a granular mixture to separate into its different components. Grains segregates in the direction of the shaking as well as transverse to it. Segregation is accomplished in vertical and horizontal vibrating chambers, and rotating cylinders. As we will see, majority of the segregation studies have been done in vertically vibrated system.

The most popular example of segregation of vertically vibrated granular materials is the ‘Brazil-nut effect’. When a box containing a number of small balls and one large ball is vibrated vertically, the large ball rises to the top irrespective of its density compared to the smaller ones as illustrated in Fig. 2.1 (Rosato et al. 1987). A horizontal Brazil-nut effect also occurs in granular systems (Schnautz et al. 2005). In a rotating circular container, light particles move towards the boundary of the container while heavier ones shift to the center.

For the Brazil-nut effect, many explanations have been proposed: percolation, convection, container’s geometry, the effect of interstitial air, and density and size ratio of the big and smaller particles. The percolation refers to the smaller particles pass through the holes created by the larger ones. Rosato et al. (1987) suggested that large particle rise to the top due to filling of voids, which are generated underneath the large particle by smaller ones in

each vibrating cycle.

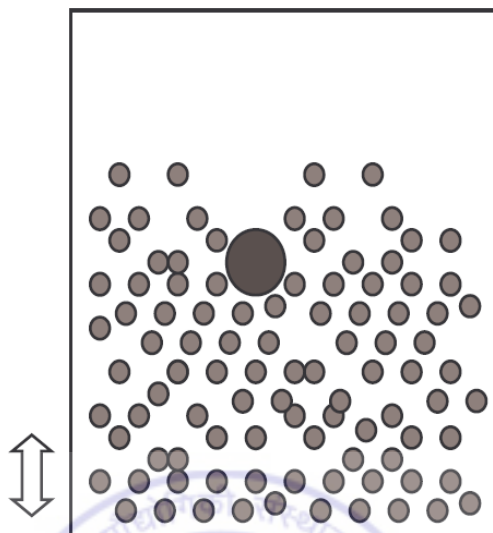


Figure 2.1: Brazil-nut effect: Large ball rising to the top

Knight et al. (1993) came up with the idea that convection drives size segregation in vertically vibrated granular mixture. They conducted an experiment for investigating the parameters that cause a single large glass bead to rise to the top through smaller glass beads in a vertically vibrated cylindrical container as displayed in Fig. 2.2. The cylindrical container was subjected to vertical taps in a time interval of one second. They observed a convection current that goes downwards along the side walls and rises to the top in the center of the cylindrical container. This convective force lift the large glass bead to the top and keeps it there if the particle size is greater than the width of the downward convection stream along the side wall. To check whether convection is induced because of the friction at interaction with the boundary wall, they extended their study by making left side of the cylinder smooth (see Fig. 2.3 (a)). It was observed that, there was no downward motion of beads along the smooth side wall of the cylindrical column as shown in Fig. 2.3 (a). Thus, it became clear that friction of the boundary walls causes a convection current in the vibrated granular system. Convection is also observed in the horizontally vibrated granular material

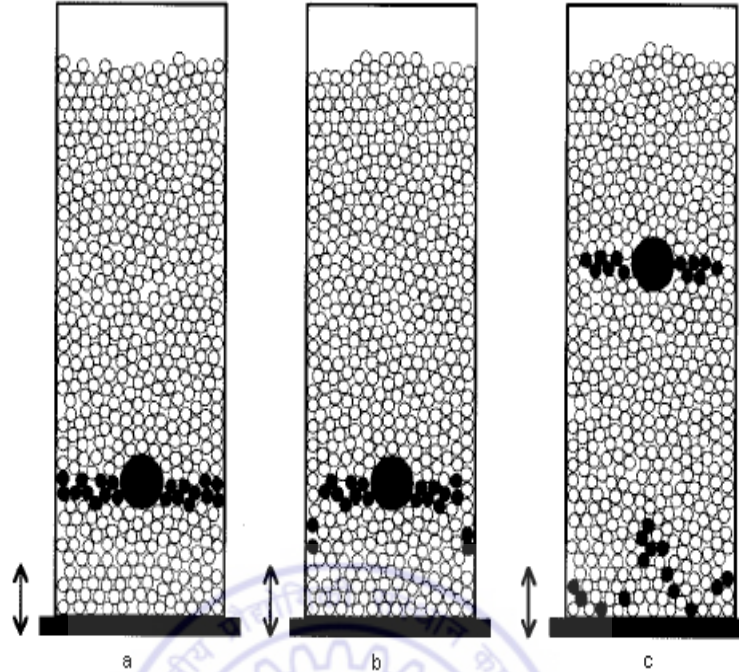


Figure 2.2: (a). Initial position of large glass bead (b). Configuration after few taps (c). Large glass bead reaches top after several taps, Knight et al. (1993)

(Medved et al. 1999) and it also depends upon the roughness of the boundary wall and geometrical dimensions, e.g., width, depth, and length of the shaker.

Effect of container geometry was also investigated by Knight et al. (1993) by employing a conical shaped container (see Fig. 2.3 (b)). The large glass bead sink to the bottom due to the reverse direction of convection current as compare to that in cylindrical container. Initially, the small black beads were at the bottom of the conical container. Fig. 2.3 (b) shows position of small black beads and large glass bead after many taps.

The effect of interstitial fluid, i.e., air, on the motion of the large particle has also been investigated experimentally by Mobius et al. (2001, 2005). It was observed that air plays an important role in the motion of large particle in a vertically vibrated granular bed. Mobius et al. in their experiment observed that the rise time of the large particle does not have a monotonic dependence on density which is in contradiction with the effect noticed earlier by

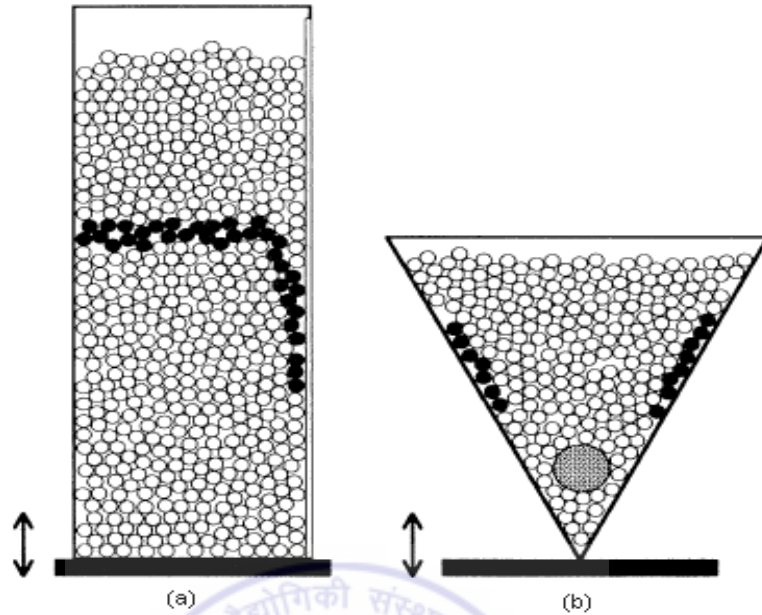


Figure 2.3: (a). Configuration of the glass beads after several taps. Black glass beads on the right side of the container reaches bottom due to the roughness of the right wall while the beads in contact with the left smooth wall doesn't get affected. (b). Positions of glass beads in a conical shaped container after several taps, Knight et al. (1993)

Shinbrot and Muzzio (1998) and Hong and Quinn (2001). The rise time depends upon the ratio of large particle's density to the surrounding smaller particles. Mobius et al. (2005) also investigated how the ambient pressure, initial position of the large particle, and convection in the granular bed affect its motion in vertically vibrated chamber.

This is not always the case that the large particle segregates to the top of the vibrating container. There are some observations for the reverse of this phenomena (Shinbrot and Muzzio 1998; Hong and Quinn 2001). This is called Reverse Brazil-nut effect. When a large grain in a deep bed of small grains is vibrated at high amplitude, the larger one sink to the bottom of the bed (Shinbrot and Muzzio 1998). Inertia was observed to be important for this effect to take place. It was also observed that, for the same granular system, tuning of some parameters may cause the large particle to sink to the bottom. The explanation presented

for the crossover from Brazil-nut effect to Reverse Brazil-nut effect was competition between the percolation effect and condensation of granular particles (Hong and Quinn 2001).

Horizontal segregation of particles is observed in a vertically vibrated granular system. It is observed that heavy grains in a mixture of small grains cluster spontaneously and undergoes horizontal segregation (Sanders et al. 2004). Fig. 2.4 shows a snapshot of a simulation in which eleven big particles of different density are vibrated with the smaller particles. It is observed that particles of approximately the same density shows a collective behavior. The high density particles sink to the bottom, while low density particles rise up to the surface. It was also observed that a stratified flow of particles in the horizontal direction occurs when they are vibrated vertically with a base of sawtooth-shaped profile (see Fig. 2.5) (Levanon and Rapaport 2001).

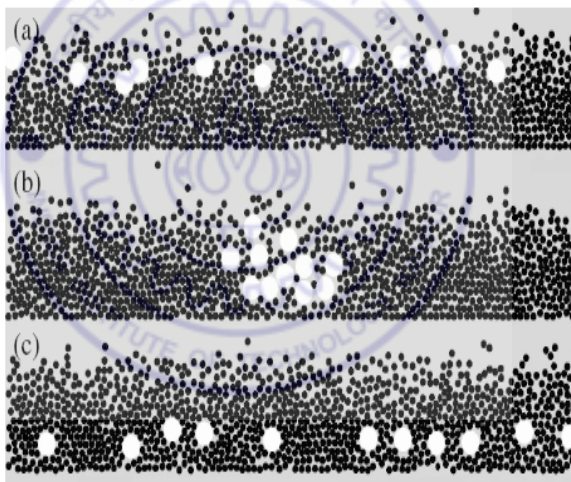


Figure 2.4: Horizontal Segregation in a vertically vibrated granular bed for different density ratios, Duncan et al. (2004)

Segregation of grains also occur in long and slowly rotating cylinders with the cylinder axis horizontal (Rapaport 2002, 2007) . This type of granular segregation has been studied extensively in experiment, in which a horizontal cylinder, partially filled with a mixture of grains, is rotated at a constant rate. Under appropriate conditions, the grains segregate into different components along the axis of the cylinder as shown in Fig. 2.6.

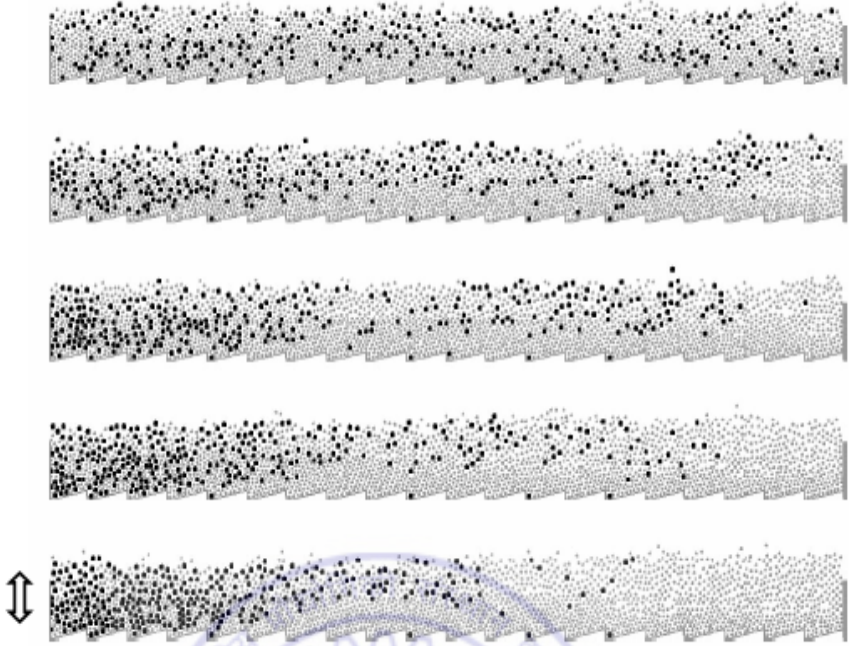


Figure 2.5: Large particles segregates horizontally in vertically vibrated granular system, Levanon & Rapaport (2001)

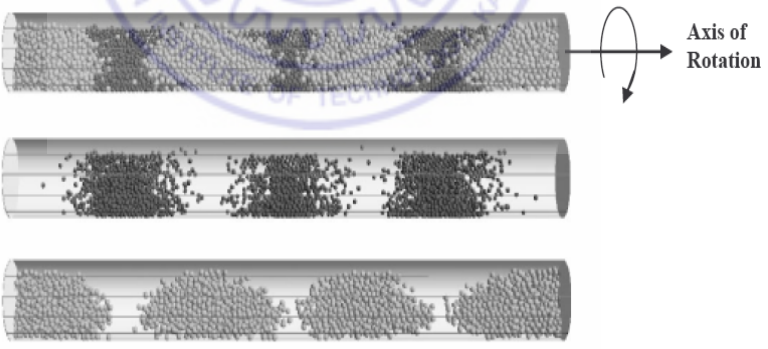


Figure 2.6: Axial segregation of grains in a rotating cylinder, Rapaport (2002)

We have reviewed vertical and horizontal segregation of grains in a vertically vibrated granular system, and observed that there are many parameters that cause segregation. These include: size, shape, density, and frictional properties of constituent particles, and their

interaction with system's boundary walls and effect of any interstitial fluid that may be present. Convection also plays an important role. It is also noticed that segregation of grains in different granular system is governed by some common parameters. By considering this fact, we also expect the influence of above discussed phenomenon and parameters in our system even with different container geometry.



Chapter 3

Simulation methodology

Granular dynamics is multi-particle dynamics. Therefore, it cannot be solved analytically. Various simulation methodologies are available for numerically evaluating the behavior of granular flows. These are: a) Molecular Dynamics (MD) simulation, b) Monte Carlo (MC) simulation, and c) Discrete element method (DEM). A detailed description of these simulation techniques is provided below.

3.1 Molecular Dynamics simulation

Molecular Dynamics simulation (Allen and Tildesley 1987; Frenkel and Smit 1996; Rapaport 2004; Poschel and Schwager 2005) is a computational experiment used primarily to study the behavior of a molecular system consist of atoms and molecules. In this simulation technique, Newton's equations of motion are integrated to find the positions of particles at discrete time intervals.

$$\mathbf{F}_i = m_i \frac{d^2 \mathbf{r}_i}{dt^2}, \quad (3.1)$$

where \mathbf{F}_i is the total force acting on the i^{th} particle, m_i is its mass and r_i is its position at time t . Orientation and angular velocity of particles are calculated by using the Euler's equations (3.2).

$$\boldsymbol{\tau} = I \boldsymbol{\alpha} + \boldsymbol{\omega} \times I \boldsymbol{\omega}, \quad (3.2)$$

where $\boldsymbol{\tau}$ is total torque acting on a particle, I is the mass moment of inertia of a particle about its center of mass, and $\boldsymbol{\alpha}$ and $\boldsymbol{\omega}$ are the angular acceleration and velocity, respectively. In case of spheres, the inertia tensor I is isotropic, i.e., $I = I \underline{\underline{1}}$, where $\underline{\underline{1}}$ is an identity matrix. So, $\boldsymbol{\omega} \times I \boldsymbol{\omega} = I \boldsymbol{\omega} \times \boldsymbol{\omega} = 0$, which reduces 3.2 to 3.3,

$$\boldsymbol{\tau} = I \boldsymbol{\alpha} . \tag{3.3}$$

Above equations are numerically integrated by employing a suitable integration algorithm. These algorithms will be discussed in detail later. A step-by-step simulation procedure is explained schematically by the flow chart in Fig. 3.1. At the first step of a simulation,

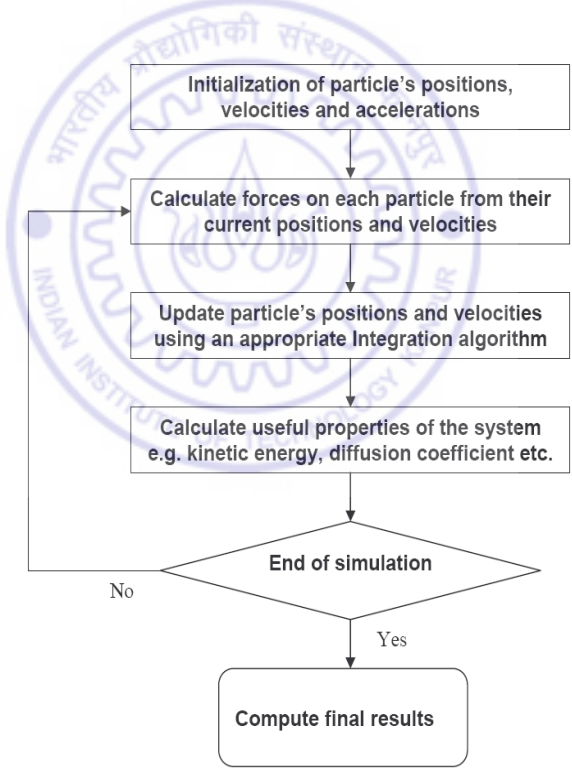


Figure 3.1: An algorithm of molecular dynamics simulation

particle's positions, velocities, and accelerations are initialized. There are several ways to generate an initial configuration. They include:

1. Arranging particles in a lattice, i.e., Face centered cubic (FCC), Body centered cubic (BCC) etc.
2. Randomly distributing the particles in the given system's domain.

Similarly, initial values of particles' velocities and accelerations can be taken as zero or random. It is important in Molecular Dynamics simulations to pick an integration time step and that is small enough to sustain the numerical stability of the simulation. This type of simulation method is also called force-based or time-driven simulation. Its applications are mainly in the field of material science, chemical engineering, and bio-molecules.

Another type of Molecular Dynamics is the event-driven Molecular Dynamics simulation (Poschel and Schwager 2005). The central idea of an event-driven Molecular Dynamics simulation is that, at any instant of time, in the entire system there occurs at most one collision of a very short duration. In contrast, multiple collisions are allowed in a force-based Molecular Dynamics simulation. It is preferable to employ event-driven Molecular Dynamics in those systems where the mean-free time of a particle is more than the collisional time between two particles. Mean-free time is the time in which a particle persists without interaction with either any other particle or with the system's boundary walls. Therefore, this technique is more useful in dilute systems like granular gases, where particles spend most of their time in free flight.

3.2 Monte Carlo simulation

Monte Carlo simulation is a probabilistic computational technique. It is very popular in molecular modeling. This method employs random numbers to generate successive configurations of system under analysis. Randomly generated configurations are accepted when particles do not overlap with each other and with the system's boundary walls. For detailed description we refer the reader to Allen and Tildesley (1987) and Poschel and Schwager (2005).

3.3 Discrete element method

Discrete Element Method (DEM) or Distinct Element Method is, like Molecular Dynamics, a deterministic technique that finds the trajectories of discrete particles. It is viewed as a generalization of the Molecular Dynamics simulation technique, in which particles can have an irregular geometrical shape. In the discrete element method, possible inelastic nature of particles may be accommodated. This method was originally employed to solve problems in rock mechanics by Cundall and Strack (1979). It is a simple, yet very useful, technique to simulate granular flows in powder technology, mining, agriculture and food industries, pharmaceutical, oil, and chemical industries.

The principle of discrete element method is to follow the trajectory and rotation of each particle while stepping forward in time. From the current position and orientation of each particle, forces and moments are calculated, that are then utilized as initial data for Newton's and Euler's equations of motion (3.1 and 3.2) to find the particle's subsequent positions and velocities at the next time step. It is assumed that over one time step the forces acting on the particle and, so the particle's acceleration, remains constant; the particle's velocity varies linearly. This makes the selection of a suitable time step very important in a particular simulation that maintains the stability and accuracy of the algorithm. Simulation algorithm in the discrete element method is the same as in the case of molecular dynamics simulation (see Fig. 3.1).

The advantage of discrete element method is its capability to simulate various phenomena in granular flows. Its limitation is that it is computationally intensive. Significant computational power is required to analyze a process completely. Therefore, it restrict us to use relatively few particles and/or small time durations.

Various types of force models are employed to model particle-particle and particle-wall interactions. A detailed description follows.

3.4 Force laws

In the present system, particles are of a spherical shape. Two particles are in contact with each other if the distance between their centers is less than the sum of their radii as illustrated in Fig. 3.2. Therefore, the mutual overlap between particles i^{th} and j^{th} is given by

$$\xi = R_i + R_j - |\mathbf{r}_i - \mathbf{r}_j| > 0, \quad (3.4)$$

where R_i , R_j are the radius, and \mathbf{r}_i , \mathbf{r}_j are the position vectors of i^{th} and j^{th} particle, respectively. To illustrate clearly the contact between two colliding grains, a two-dimensional picture is drawn, as shown, in the Fig. 3.2, where $\hat{\mathbf{r}}_{ij}$ is the unit vector along the line

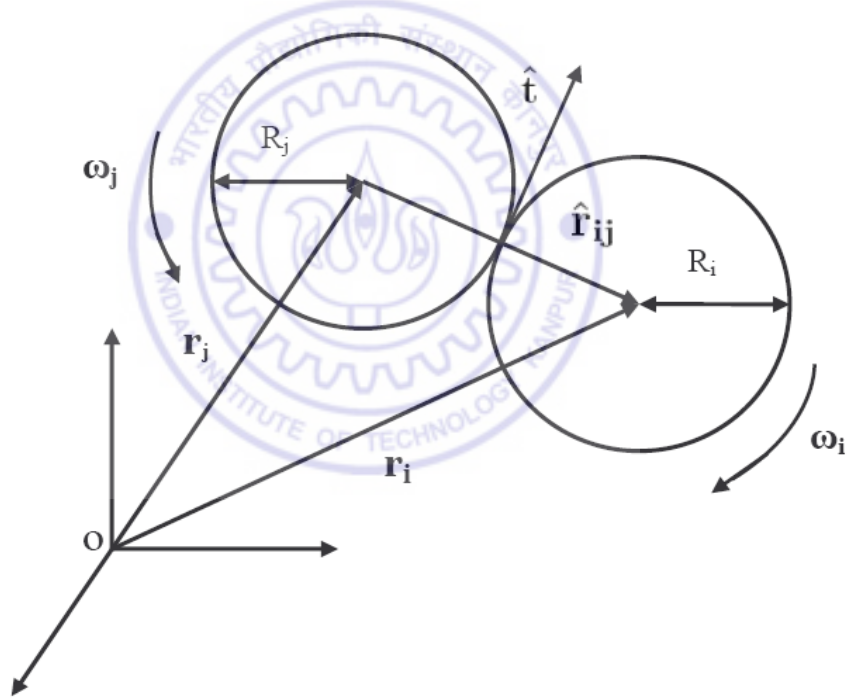


Figure 3.2: Contact between two particles

connecting centers from j^{th} to i^{th} particle, $\hat{\mathbf{t}}$ is the unit vector along tangential direction, and ω_i and ω_j are the angular velocities of particles. The advantage of using spherical particles is that contact between two particles may be detected easily and efficiently.

Because of the inelastic nature of the interactions between granular particles, a part of their kinetic energy is lost as heat during a collision. This dissipated energy raises the temperature of the particles that can, however, be neglected. This is because thermal energy is usually much smaller than the gravitational potential energy required to lift a grain over another grain (Kudrolli 2004). Therefore, change in grains' properties due to temperature variation cannot be observed. The deformation of the particles is taken to be small, and we further assume there is no distortion in the shape of particles after many collisions.

During collision, particles experience forces in the normal $\hat{\mathbf{r}}_{ij}$ and tangential $\hat{\mathbf{t}}$ directions as shown in the Fig. 3.2. A detailed description of normal and tangential forces follows next.

3.4.1 Normal force

Normal force on a particle has two components; one due to elasticity and the other one due to dissipation (see Fig. 3.3 (a)). Thus,

$$\mathbf{F}^n = \mathbf{F}_{el}^n + \mathbf{F}_{diss}^n, \quad (3.5)$$

where \mathbf{F}_{el}^n is the normal elastic force and \mathbf{F}_{diss}^n is the normal dissipative force.

The normal force between two particles depends upon the type of force model employed in the simulation. The commonly used force models for interactions are:

1. Linear spring dashpot force model
2. Hertzian contact force model with viscous damping

Normal elastic force and dissipative force for each force model are described separately in next sections.

3.4.1.1 Normal elastic force

In linear spring force model, an interaction between two particles is assumed to be linear elastic. Normal elastic force on the i^{th} particle is thus,

$$\mathbf{F}_{el}^n = k^n \xi \hat{\mathbf{r}}_{ij}, \quad (3.6)$$

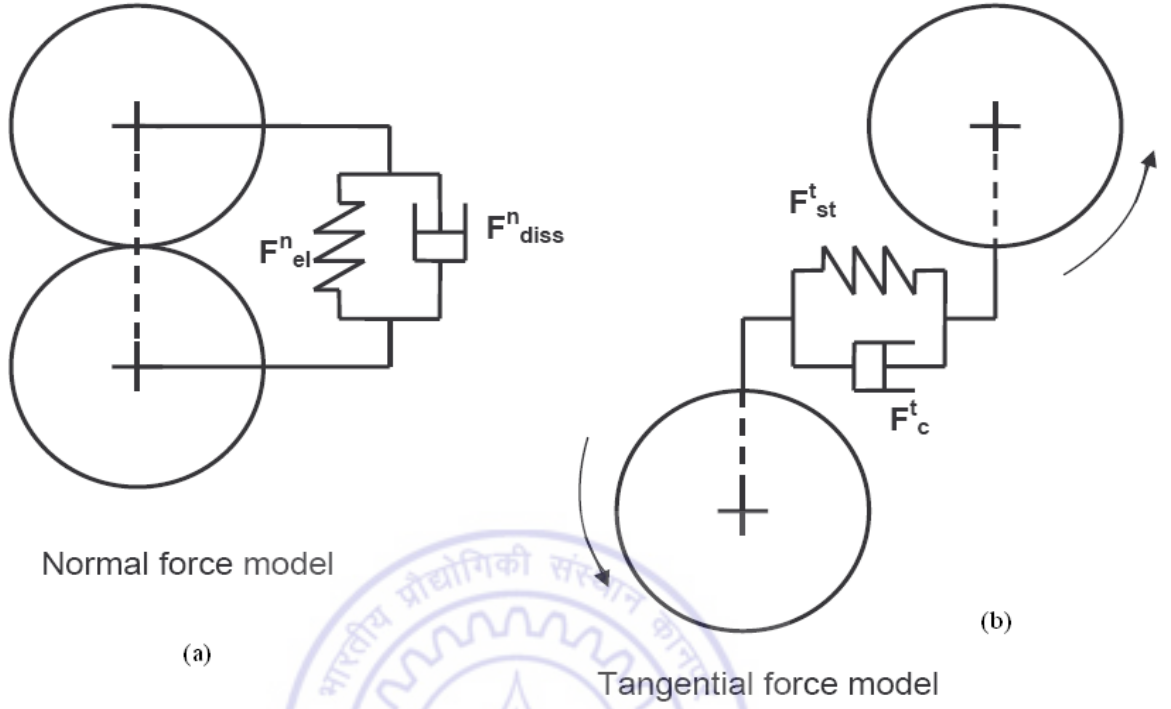


Figure 3.3: Schematic of force model

where k^n is the stiffness of a linear spring and ξ is the mutual compression of colliding particles (3.4), and $\hat{\mathbf{r}}_{ij}$ is the unit vector along the line connecting centers from j^{th} to i^{th} particle (see Fig. 3.2).

The Hertzian contact force model was derived by Heinrich Hertz (Johnson 1985) as a function of ξ and the material parameters Young's modulus Y and Poisson ratio ν . The restoring normal elastic force between two contacting spheres of the same material is given by

$$\mathbf{F}_{el}^n = \frac{2Y\sqrt{R^{eff}}}{3(1-\nu^2)}\xi^{3/2}\hat{\mathbf{r}}_{ij}, \quad (3.7)$$

where R^{eff} is the effective radius of the two colliding spheres obtained by the relation

$$\frac{1}{R^{eff}} = \frac{1}{R_i} + \frac{1}{R_j}. \quad (3.8)$$

In case of particles of different materials, 3.7 will be modified to 3.9,

$$\mathbf{F}_{el}^n = \frac{4\sqrt{R^{eff}}}{3} \left(\frac{1 - \nu_i^2}{Y_i} + \frac{1 - \nu_j^2}{Y_j} \right)^{-1} \xi^{3/2} \hat{\mathbf{r}}_{ij}, \quad (3.9)$$

where Y_i and Y_j are Young's modulus, and ν_i and ν_j are Poisson ratio for the i^{th} and j^{th} particle, respectively.

In addition to the above two force models, normal elastic force between two particles can also be modeled through Lennard-Jones potential.

The repulsive force due to a Lennard-Jones potential (see Fig. 3.4) can also be implemented as a short-range force (see Fig. 3.5) to model inter-particle interaction. It has been used successfully by some researchers in their study of granular materials, e.g., Rapaport (2004). A truncated Lennard-Jones force model is employed by introducing a cut-off range to incorporate the fact that no interaction takes place between non-contacting grains. The Lennard-Jones force within the cut-off range between particles located at \mathbf{r}_i and \mathbf{r}_j with diameters σ_i and σ_j , respectively, is

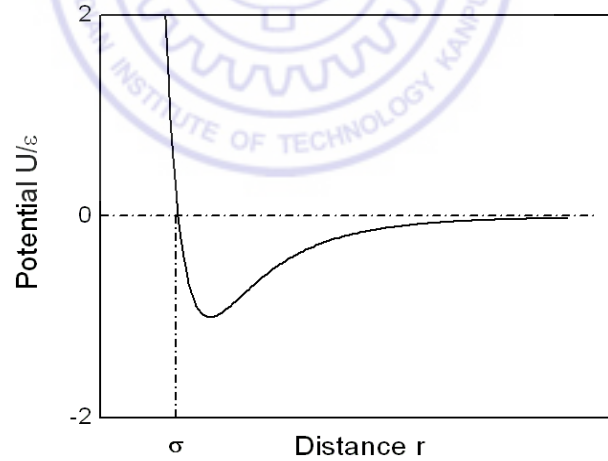


Figure 3.4: Lennard-Jones Potential with the distance between particles

$$\mathbf{F}_{el}^n = \frac{48}{r_{ij}} \left(\left(\frac{\sigma_{ij}}{r_{ij}} \right)^{12} - 0.5 \left(\frac{\sigma_{ij}}{r_{ij}} \right)^6 \right) \hat{\mathbf{r}}_{ij}, \quad (3.10)$$

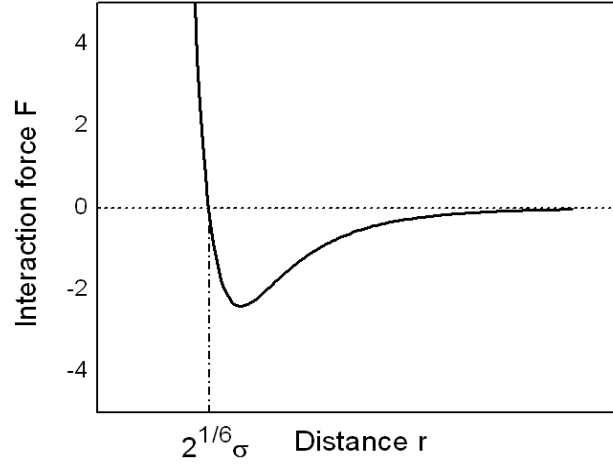


Figure 3.5: Variation of Lennard-Jones force with the distance between particles

where $r_{ij} = |\mathbf{r}_i - \mathbf{r}_j|$ is the distance between the center of two particles, $\sigma_{ij} = (\sigma_i + \sigma_j)/2$ is the mean diameter of two particles, and $\hat{\mathbf{r}}_{ij}$ is the location of i^{th} particle with respect to j^{th} particle. We take the cut-off distance to be $r_{cut} = 2^{1/6}\sigma_{ij}$, as it is clear from the Fig. 3.5 that the interaction force becomes negative, which indicates attraction between grains, above this cut-off distance. As, grains do not attract, so, this cut-off distance allows the particles to have only repulsive forces.

3.4.1.2 Normal dissipative force model

Here, we will discuss two dissipative force models; one has linear dependence on particles' deformation rate and the other one has dependency on particles' mutual deformation along with their deformation rate.

In the first case, the normal dissipative force is assumed to be of the form,

$$\mathbf{F}_{diss}^n = -\gamma^n m^{eff} (\mathbf{v}_{ij} \cdot \hat{\mathbf{r}}_{ij}) \hat{\mathbf{r}}_{ij}, \quad (3.11)$$

where $\mathbf{v}_{ij} = \mathbf{v}_i - \mathbf{v}_j$ is the relative velocity of the i^{th} particle with respect to the j^{th} particle, $\mathbf{v}_{ij} \cdot \hat{\mathbf{r}}_{ij}$ is the component of relative velocity along the line connecting centers, γ^n is the normal

damping coefficient, and $m^{eff} = m_i m_j / (m_i + m_j)$ is the effective mass of two particles.

For inelastic collisions, the coefficient of restitution ε can be taken as a parameter for energy loss. It is the ratio of normal relative velocity of particle just after and just before a collision.

$$\varepsilon = -v_{after} / v_{before}, \quad (3.12)$$

where v_{before} , v_{after} is the relative velocity of particle before and after collision.

Because collision do not create energy, the coefficient of restitution always lies between 0 and 1, where a unit value corresponds to energy-preserving perfectly elastic collision, and zero value to the case when particles stick to each other post-collision. For the present force model, normal damping coefficient γ^n and coefficient of restitution ε relate to each other (Ristow 1994) by

$$\gamma^n \approx -\frac{\ln \varepsilon}{\sqrt{\pi^2 + \ln^2 \varepsilon}}. \quad (3.13)$$

It is clear from the above equation that ε is independent of the impact velocity of colliding particles. However, experimental investigations have suggested the dependence of coefficient of restitution on the impact velocity. This is because of the non-linear damping. However, we will for the moment overlook this non-linearity.

In the second dissipation force model, the normal dissipative force depends upon the deformation ξ , and its rate $\dot{\xi}$ of colliding particles. It is given by

$$\mathbf{F}_{diss}^n = \frac{2Y\sqrt{R^{eff}}}{3(1-\nu^2)} A \sqrt{\xi} \dot{\xi} \hat{\mathbf{r}}_{ij}, \quad (3.14)$$

where Y is Young's modulus, R^{eff} is the effective radius of two colliding particles and is given by 3.8, ν is the Poisson ratio, A is dissipative constant and a function of material viscosity (Brilliantov et al. 1996), and $\hat{\mathbf{r}}_{ij}$ is unit vector along the line connecting centers from j^{th} to i^{th} particle.

For the particles having different materials, 3.14 will be modified to 3.15

$$\mathbf{F}_{diss}^n = \frac{4\sqrt{R^{eff}}}{3} \left(\frac{A_i + A_j}{2} \right) \dot{\xi} \sqrt{\xi} \hat{\mathbf{r}}_{ij}, \quad (3.15)$$

where A_i and A_j are dissipative constants for i^{th} and j^{th} particle.

3.4.2 Tangential force

In an oblique collision, a tangential force acts between the particles in addition to their normal interaction. This force depends on the surface properties of the granular particles. Due to friction between the particle's surfaces, a tangential force acts which in turn rotates the particles. \mathbf{v}_{ij}^t is the component of relative velocity along the tangential direction $\hat{\mathbf{t}}$ as illustrated in Fig. 3.2. This is given by

$$\mathbf{v}_{ij}^t = \mathbf{v}_{ij} - (\hat{\mathbf{r}}_{ij} \cdot \mathbf{v}_{ij}) \hat{\mathbf{r}}_{ij} - \left(\frac{\sigma_i \boldsymbol{\omega}_i + \sigma_j \boldsymbol{\omega}_j}{\sigma_i + \sigma_j} \right) \times \mathbf{r}_{ij}, \quad (3.16)$$

where $\boldsymbol{\omega}_i, \boldsymbol{\omega}_j$ are angular velocity of i^{th} and j^{th} particle.

The tangential force is given by

$$\mathbf{F}^t = -\min(\mu |\mathbf{F}^n|, \gamma^t |\mathbf{v}_{ij}^t|) \hat{\mathbf{v}}_{ij}^t, \quad (3.17)$$

where $\min(a, b)$ is minimum of a and b , γ^t is the tangential damping coefficient, static friction coefficient μ sets an upper bound proportional to $|\mathbf{F}^n|$ according to Coulomb's law. The above tangential force is simply a less singular version of the classical dry Coulomb friction model, as shown in the Fig. 3.6

Though the above force law is used very widely, it has certain limitations. This law is reliable in those granular flows where colliding particles have finite velocities. It is not suitable for static granular systems because a zero relative tangential velocity will predict zero tangential force, which may result in the collapse of the granular structure. Also, an experimental investigation tells that the tangential elasticity exists that can reverse the tangential velocity of particles. The model proposed by Cundall and Strack (1979) helps to overcome this difficulty. When two particles comes into contact, a tangential spring acts between their contact points, which can elongate and shorten while the particles are in contact with each other (see Fig. 3.3 (b)). Its elongation or compression is given by

$$\zeta(t) = \int_{t_0}^t v_{ij}(t') dt', \quad (3.18)$$

where t_0 is the time at which two particles came into contact. This tangential force is again

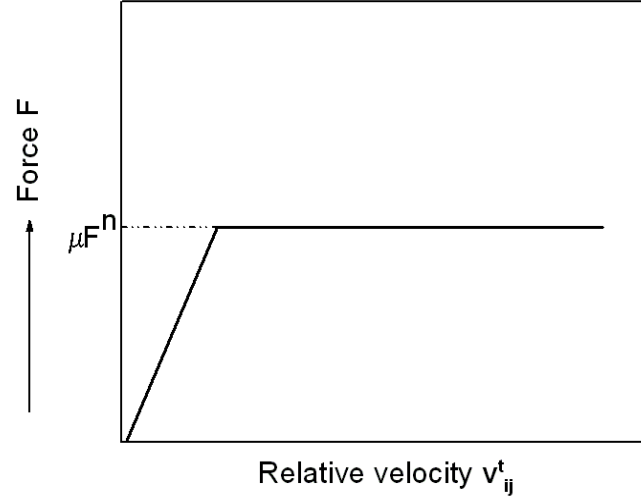


Figure 3.6: Coulomb friction model: A limiting friction force to prevent sliding occur between particles

limited by the coulombs' friction law.

$$\mathbf{F}^t = -\min(\mu |\mathbf{F}^n|, |k^t \zeta|) \hat{\mathbf{v}}_{ij}^t. \quad (3.19)$$

It is important to note that the system behavior does not depend on the type of force model used. This is verified by us in our present vibrating granular system by comparing the results from a Hertzian contact force model with those from a Lennard-Jones force model.

We are employing Hertzian contact force model (3.7) along with linear dissipative force model (3.11) for interactions between particles in our simulation. Tangential forces are implemented by using the model given by 3.17. These force laws are employed for both particle-particle and particle-wall interactions. The particles' interaction with the channel's walls is implemented in such a way that when a grain comes within the cut-off range of a wall, a virtual granular particle is created at the foot of the perpendicular (see Fig. 3.7) dropped from the colliding grain on to the wall.

This latter construction ensures that the radial force experienced by the incoming grain is indeed normal to the wall, as should be the case. Here, we assume that this virtual

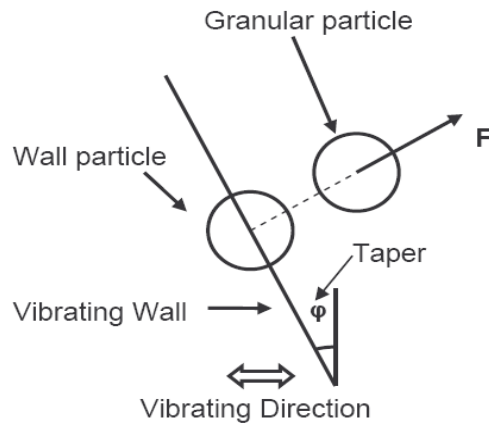


Figure 3.7: Particle interaction with system's boundary wall

particle has similar properties to the ones in the mixture. This is a simplifying, but not necessary, assumption. The colliding grain now interacts with the wall particle according to the collisional framework developed above for particle-particle interaction.

As dry granular particles do not attract each other, we set normal force to be zero whenever it becomes negative (Poschel and Schwager 2005).

3.5 Integration algorithm

There are various integration algorithms for numerically integrating the equations of motions of granular particles (Allen and Tildesley 1987). The popular algorithms for calculating trajectories of particles are:

1. Verlet algorithm
2. Leapfrog algorithm,
3. Velocity Verlet algorithm

As Allen and Tildesley (1987) state, the desirable characteristics of a successful simulation algorithm are:

1. "It should be fast, and require little memory.
2. It should permit the use of a long time step δt .

3. It should duplicate the classical trajectory as closely as possible.
4. It should satisfy the known conservation laws for energy and momentum, and be time-reversible
5. It should be simple in form and easy to program”.

We now describe the three algorithm listed above.

3.5.1 Verlet algorithm

The Verlet algorithm calculates the position of a particle at time $t + \delta t$ by using its position and acceleration at the present time t and the position at the previous time $t - \delta t$, where δt is the integration time step. It does not make use of velocities. It is derived by using Taylor expansion series to make forward and backward expansions in time of a particles' position coordinates $\mathbf{r}(t)$, viz.,

$$\mathbf{r}(t + \delta t) = \mathbf{r}(t) + \mathbf{v}(t)\delta t + \frac{\mathbf{a}(t)\delta t^2}{2!} + O(\delta t^3) \quad (3.20)$$

$$\text{and } \mathbf{r}(t - \delta t) = \mathbf{r}(t) - \mathbf{v}(t)\delta t + \frac{\mathbf{a}(t)\delta t^2}{2!} - O(\delta t^3), \quad (3.21)$$

where \mathbf{v} and \mathbf{a} are the velocity and acceleration of a particle. Adding the above two equations yields the Eqn. 3.22, which is used in advancing positions of particles in Verlet algorithm.

$$\mathbf{r}(t + \delta t) = 2\mathbf{r}(t) - \mathbf{r}(t - \delta t) + \mathbf{a}(t)\delta t^2 + O(\delta t^4). \quad (3.22)$$

Velocities are calculated from the positions of particles at a previous and a future time step by

$$\mathbf{v}(t) = \frac{1}{2\delta t} [\mathbf{r}(t + \delta t) - \mathbf{r}(t - \delta t)]. \quad (3.23)$$

Implementation of the above equations in a simulation is shown schematically by the flow chart in Fig. 3.8.

Characteristics of the Verlet algorithm are:

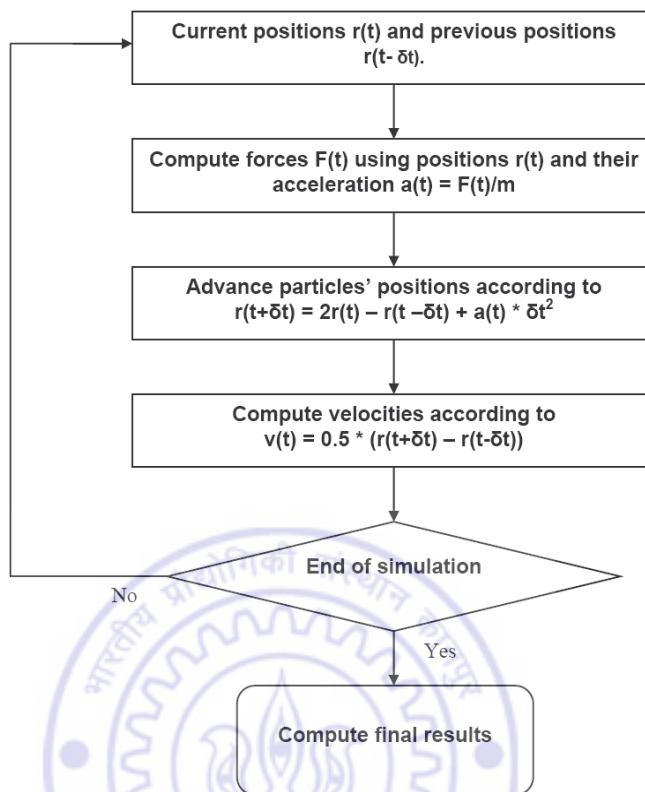


Figure 3.8: Schematic of Verlet algorithm in simulation

1. The Verlet algorithm is reversible in time, i.e., if we put $-\delta t$ in place of δt in 3.22, the same equation will come out. It shows that the particles' trajectories can be retraced backward in time
2. With large time steps, this algorithm shows good energy conservation properties

Limitations associated with this algorithm are:

1. Handling of velocities is not efficient because velocity at time t is calculated when positions are available at time $t + \delta t$
2. Numerical imprecision is also associated because of addition of $O(\delta t^2)$ small and large quantities $O(1)$ as illustrated by 3.22.

3.5.2 Leapfrog algorithm

The leapfrog algorithm is a modified version of the Verlet algorithm. Here, the position of a particle at time $t + \delta t$ is calculated from its position at time t and its velocity at time $t + \frac{\delta t}{2}$, i.e.,

$$\mathbf{v}(t + \frac{1}{2}\delta t) = \mathbf{v}(t - \frac{1}{2}\delta t) + \mathbf{a}(t)\delta t \quad (3.24)$$

$$\text{and } \mathbf{r}(t + \delta t) = \mathbf{r}(t) + \mathbf{v}(t + \frac{1}{2}\delta t)\delta t \quad . \quad (3.25)$$

The velocity of particle at time t can also be computed by taking the average of the velocities at time $t + \frac{1}{2}\delta t$ and $t - \frac{1}{2}\delta t$:

$$\mathbf{v}(t) = \frac{1}{2} \left[\mathbf{v}(t + \frac{1}{2}\delta t) + \mathbf{v}(t - \frac{1}{2}\delta t) \right] \quad . \quad (3.26)$$

Implementation of the above equations in a simulation is shown schematically in the flow chart of Fig. 3.9. Mathematically, this algorithm is equivalent to the Verlet algorithm. This algorithm is time reversible and, also, velocities appear explicitly while updating positions of particles. Numerical error is reduced because we do not take difference of two large quantities to obtain a small one.

3.5.3 Velocity Verlet algorithm

The Velocity Verlet algorithm computes the particle's position at a future time $t + \delta t$ by using its position, velocity and acceleration at only the present time t . The particle's velocity at time $t + \delta t$ is updated from its velocity at time t and its acceleration at times t and $t + \delta t$, viz.,

$$\mathbf{r}(t + \delta t) = \mathbf{r}(t) + \mathbf{v}(t)\delta t + \frac{1}{2}\mathbf{a}(t)\delta t^2 \quad (3.27)$$

$$\text{and } \mathbf{v}(t + \delta t) = \mathbf{v}(t) + \frac{1}{2}[\mathbf{a}(t) + \mathbf{a}(t + \delta t)] \quad . \quad (3.28)$$

The velocity Verlet algorithm is shown schematically in flow chart in Fig. 3.10

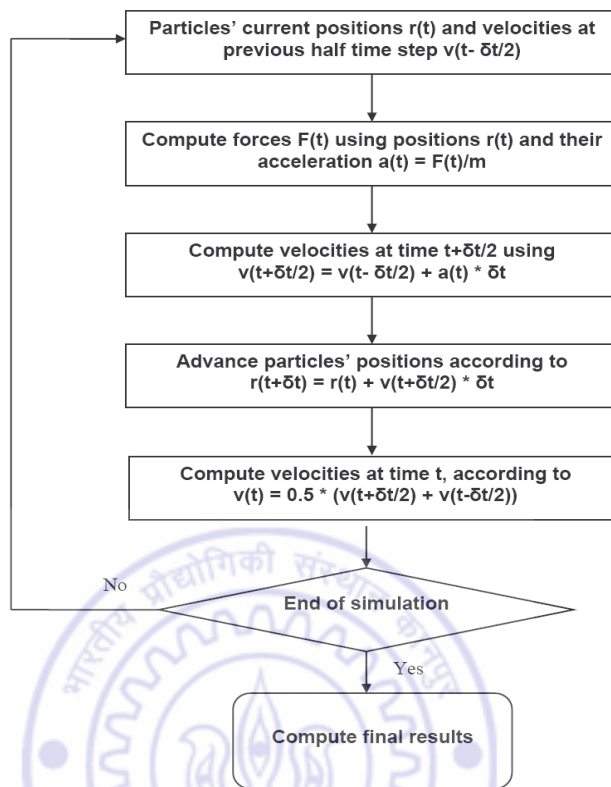


Figure 3.9: Schematic of Leapfrog algorithm in a simulation

This algorithm updates velocities in an excellent way. Positions, velocities, and accelerations are all stored at the same time t , which reduces the round-off error. We are employing velocity Verlet algorithm in our simulation because of its advantages described above.

An algorithm for molecular dynamics simulation is illustrated in Fig. 3.1. A brief description of each step is provided in next section.

3.6 Our simulation algorithm

Initialization:

The two different ways to generate an initial configuration of particles are discussed in Section

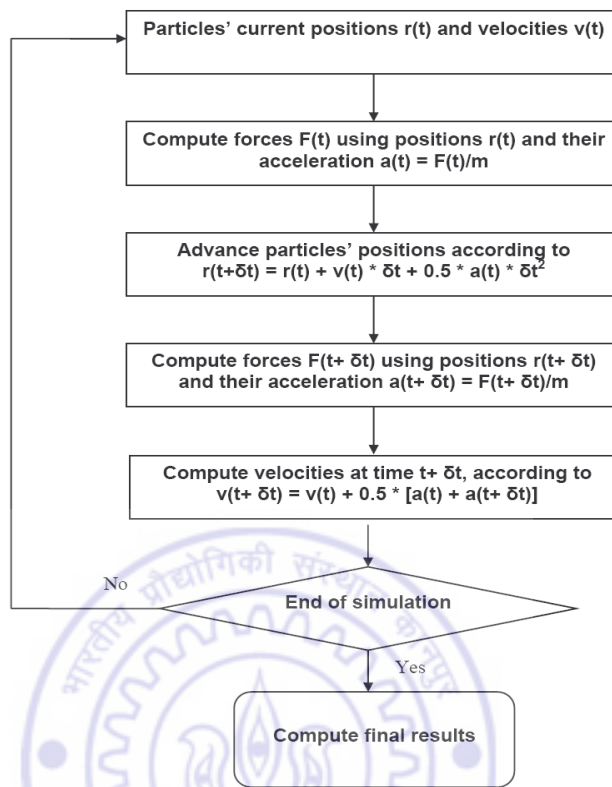


Figure 3.10: Schematic of Velocity Verlet algorithm in a simulation

3.1. However, in our simulations, we generated an initial configuration by first arranging the particles on the top of the vibrating channel (see Fig. 3.11) and then letting them fall into it under gravity (Poschel and Schwager 2005). The configuration obtained as shown in the Fig. 3.12 is used in simulations as the initial configuration. The initial values of particles' velocities and accelerations can be taken as zero or random.

Contact detection and force calculation: The contact between two particles is identified when the distance between their centers is less than the sum of their radii (Eqn. 3.2).

Updating particles' positions and velocities: Particles' positions and velocities are updated by implementing velocity Verlet algorithm. This algorithm has been described in detail in Section 3.5.

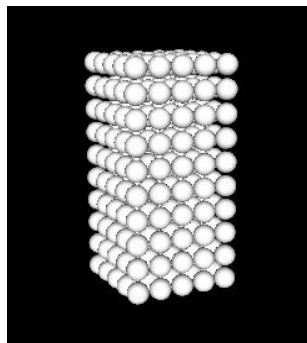


Figure 3.11: Three-dimensional view of particles arranged on top of the channel

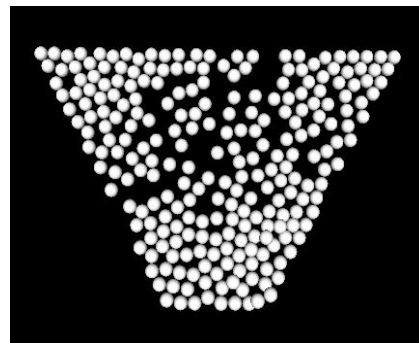


Figure 3.12: Top view of configuration of particles after dropping into the channel

Particle insertion: In our system, particles escape from the top and bottom of the inclined channel. Particles are inserted randomly in a fixed volume above the base of the vibrating channel. This randomly inserted particle is taken into the system if it does not overlap with other particles and system's boundary walls.

Time step selection: As Mishra (2003) state, "the time step for numerical integration should be set smaller than a critical value to make the calculation stable. Based on the characteristic natural frequency of a spring-mass oscillation system, the oscillation period can be calculated as $\delta t = 2\pi \sqrt{m/K}$, where m is the mass and K is the stiffness of the spring-mass system." This is the critical time step for a given material of particles used in DEM simulation. In order to resolve all collisions between particles, the time step employed should not be greater than the critical time step. We have used the time step less than its critical value. However, we haven't compared the mean collision time with our assumed time step.

In our system a particle can have contact with more than two particles at a time. However, in case of event-driven simulation only one collision takes place in the entire system. To check the code's accuracy, some verification tests has been done. These tests are discussed next.

Chapter 4

Validation tests for DEM code

Our three-dimensional DEM code is written in Fortran 90 language. We employ a Hertzian contact force model (Eqn. 3.7) to idealize contact of particles in our system. During collision, dissipation is accommodated by introducing a normal damping (Eqn. 3.11) and a tangential force (Eqn. 3.17). This force model has been discussed in detail in the previous chapter. These force laws are employed for both particle-particle and particle-wall interactions. For integrating the equations of motion of particles, the velocity Verlet integration scheme has been implemented. We have also made assumptions about our simulated granular system. These are:

1. Particles are of a spherical shape
2. Shape of the grains remains conserved after collision
3. Temperature rise in the grains after collision is negligible
4. There is no effect of interstitial air on the dynamics of granular particles.

Various tests has been done to check the accuracy of the code. In addition, the outcome has been compared with experimental data from previous research. These tests are discussed next.

4.1 Acceleration of a particle rolling down an inclined plane

These are very basic tests for testing a granular dynamics code. In these tests, a particle is allowed to move down an inclined plane under different damping conditions.

In the first case, all kind of damping and friction in the system is kept zero. In this situation, when there is no damping in the system, only sliding motion of particle occurs. Thus, the particle must slide down with an acceleration of $g \sin \theta$, where θ is the vibrating channel's inclination with the ground.

In the second test under this category, damping and frictional forces are switched on. Due to friction, particle *rolls* down with an acceleration of $5g \sin \theta/7$.

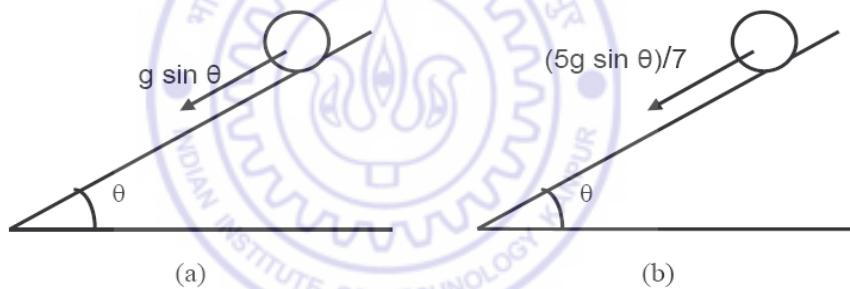


Figure 4.1: Sphere rolling down an inclined channel (a) No damping in the system (b) System with finite damping

4.2 Particle-particle or particle-wall forces

This test simulates free falling particle's interaction with the vibrating channel's base. This test is also conducted with different damping conditions. These validation tests are matched with the results given by Asmar et al. (2004). In these tests, the vibrating channel is not

inclined with the ground.

4.2.1 Zero damping

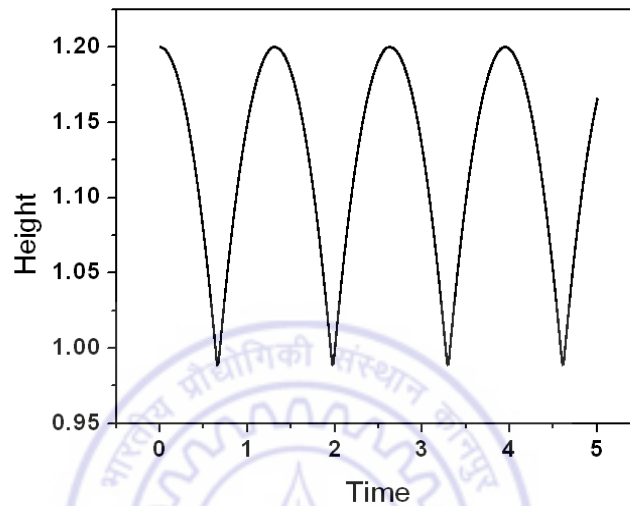


Figure 4.2: Height of particle from the surface vs time. Height is in multiples of particle diameter and time is non-dimensionalized so that one unit of simulation time approximately equals to 0.018 s.

In zero damping conditions, particle rebounds to same height after colliding with the channel's base (see Fig. 4.2). Also, as expected, the same normal force acts on the particle during successive interactions (see Fig. 4.3).

4.2.2 Finite damping

When there is some damping present in the system, the particle loses a fraction of its kinetic energy during a collision, and, so, does not rebound to the same height (see Fig. 4.4). Therefore, the velocity with which a particle collides with the channels' base decreases with time, and so does the normal elastic force during a collision (see Fig. 4.5).

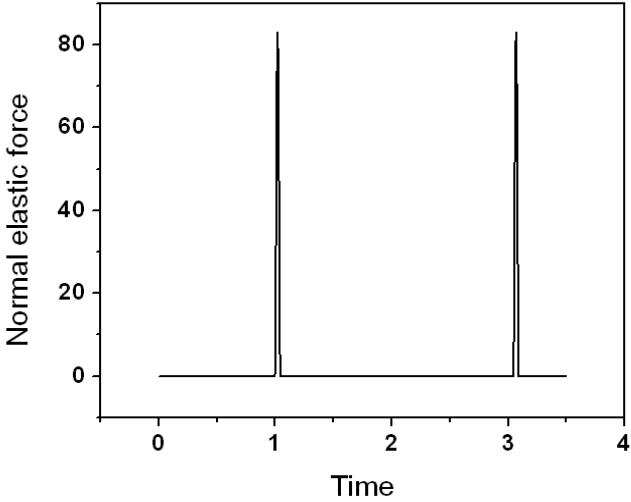


Figure 4.3: Normal elastic force on a particle by channel’s base vs time. Normal force is also non-dimensionalized by the particle’s mass, and the acceleration due to gravity.

The normal damping force experienced by the particle on successive interactions is shown in Fig. 4.6. It is also observed in Fig. 4.6 that the normal damping force is negative. This thing happens when particle starts separating from the surface because of positive $\hat{\mathbf{r}}_{ij} \cdot \mathbf{v}_{ij}$ value in separation which gives negative damping force.

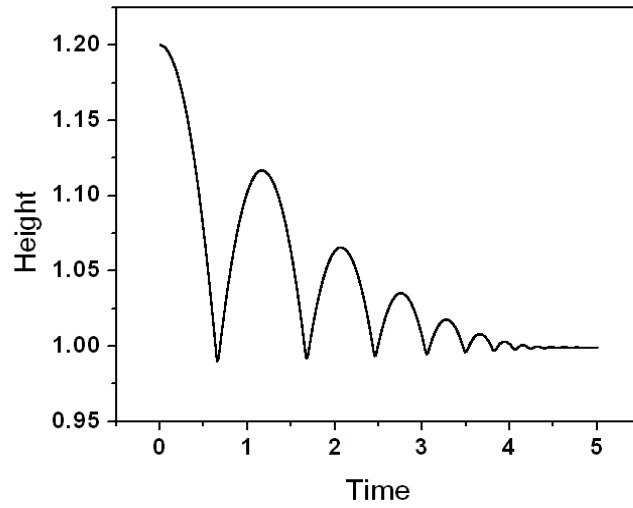


Figure 4.4: Height of particle from the channel's base vs time. Particle come to rest after collisions with the channel's base in infinite time.

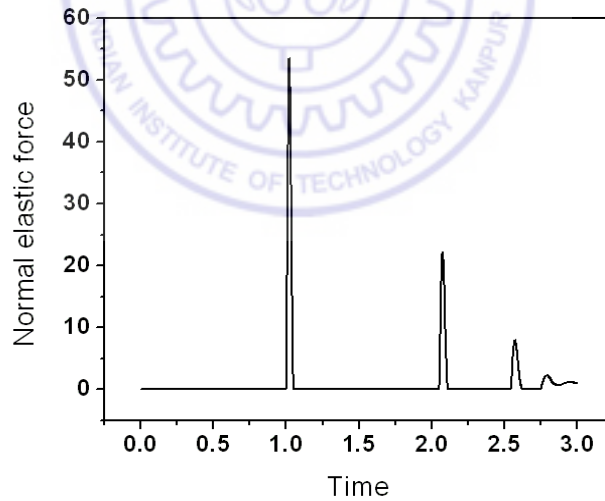


Figure 4.5: Normal elastic force on a particle by the channel's base vs time.

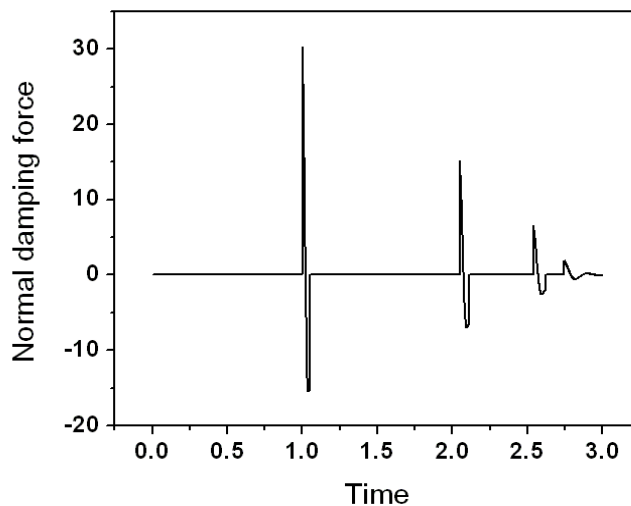


Figure 4.6: Normal damping force vs time

4.3 Vibrating channel with parallel side walls and zero inclination

In this test, vibrating channel's side walls are made parallel, and there is no inclination with the ground. This vibrating channel is open from both sides A and B as shown in the Fig. 4.7. When granular particles, in this geometrical arrangement, are vibrated horizontally, then same flow rate of particles is obtained from each side A and B.

Therefore, net flow rate of particles is zero at all vibration frequencies (see Fig. 4.8). Net flow rate is the difference between the flow rate of the particles from each side A and B. This test also gives us confidence in the accuracy of our code. It is observed from Fig. 4.8 that the flow rate from each side increases with the vibration frequency. The reason for this needs to be investigated in detail.

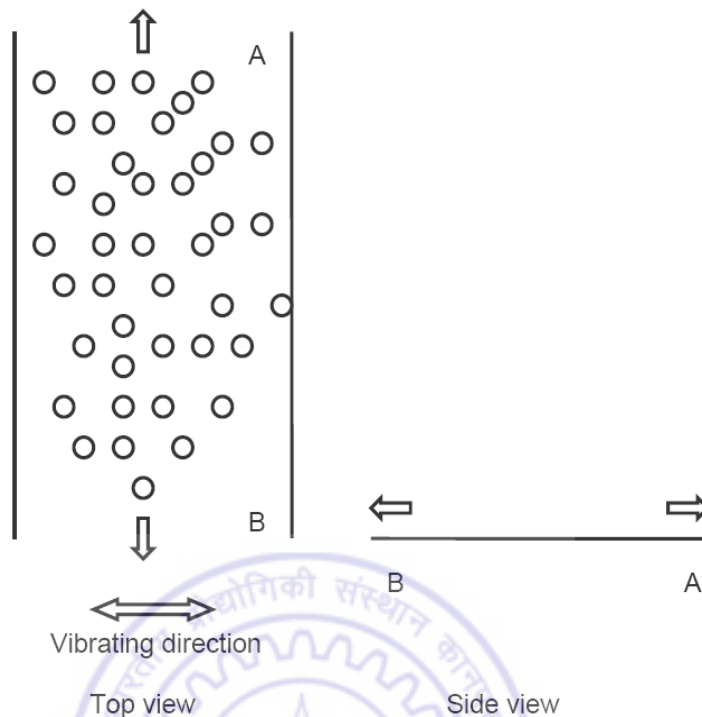


Figure 4.7: Top and side view of a vibrating channel with parallel side walls and zero inclination

4.4 Vibrating channel with parallel side walls and inclination

In this test, vibrating channel also have some inclination θ with the ground, and vibrated in an inclined direction as illustrated in Fig. 4.9. This geometrical set-up is similar with that employed by Blair and Kudrolli (2003) in their experiment. The parameters, geometrical dimensions of the vibrating channel, its inclination with the ground, size and shape of the particles, vibration amplitude and frequency, are the same with those used in the experiment mentioned above except material of the granular particles. In our simulation, we have employed rubber balls instead of steel balls to avoid numerical instability because of steel's high stiffness.

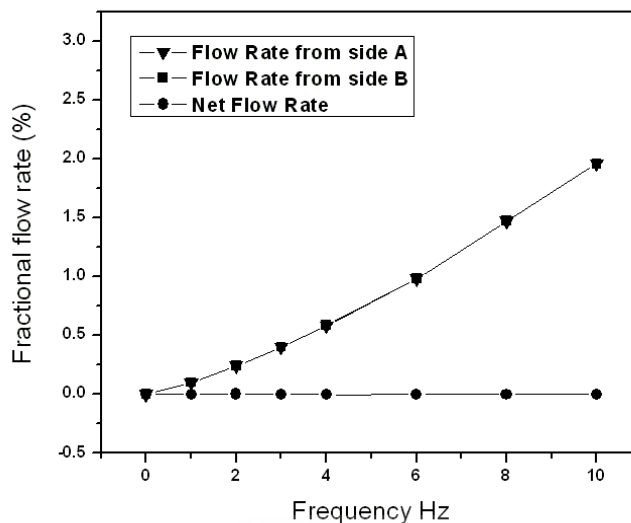


Figure 4.8: Fractional and net flow rate of particles in a vibrating channel with parallel side walls and zero inclination

The density distribution of particles from simulations is compared with their experimental counterpart. Because of different material properties of granular particles in the simulations, we only expect a qualitative match with the experiment. The density distribution is calculated both along the direction of vibration (Z), and transverse (X) to it. Figures 4.10 and 4.11 illustrate density profiles in a direction transverse to the vibration obtained from our simulation and from the experiment of Blair and Kudrolli (2003), respectively. Similarly, Figs. 4.12 and 4.13 shows the density distribution along the direction of vibration obtained from our simulation and by Blair and Kudrolli (2003), respectively. It is observed from Fig. 4.12 that variation in density distribution is qualitatively similar to the experimental observation shown in Fig. 4.13, except for the last case of 500 number of particles and 4° inclination angle. This deviation may be due to statistical error; longer runs are required, for calculating the particles' density distribution.

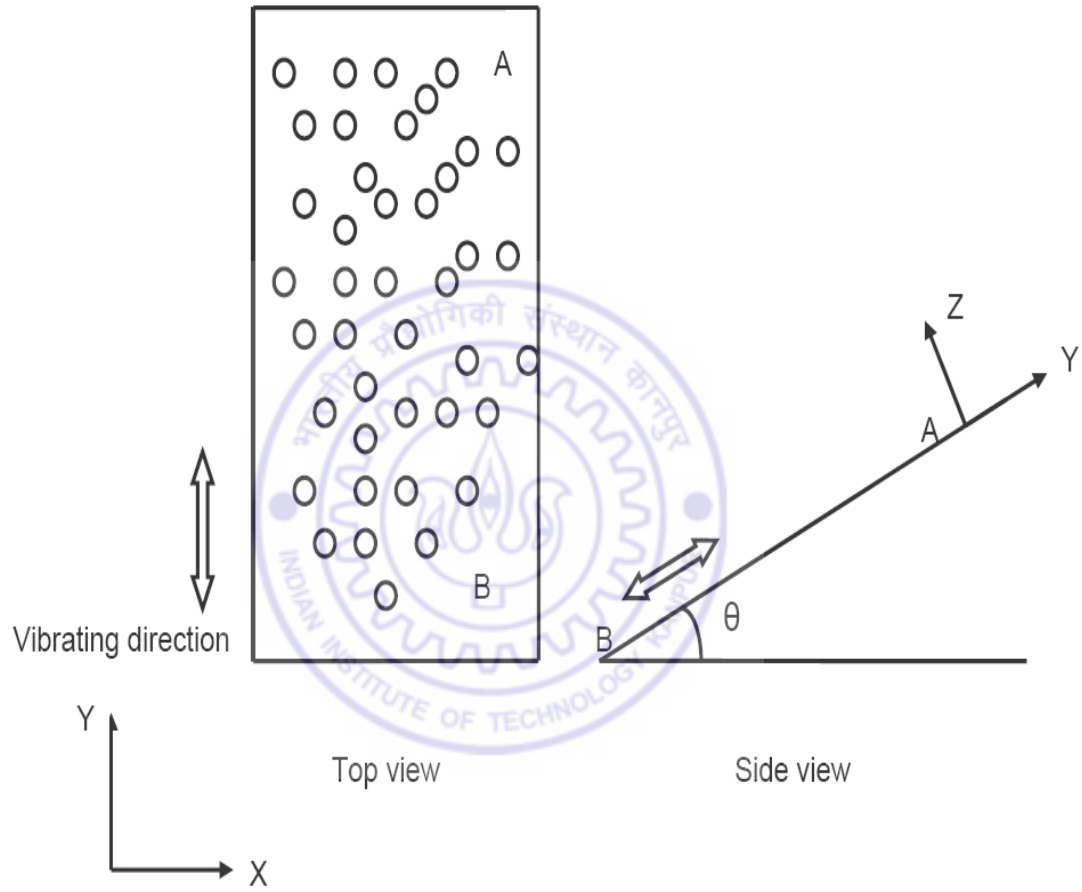


Figure 4.9: Top and side view of a vibrating channel with parallel side walls and inclination θ

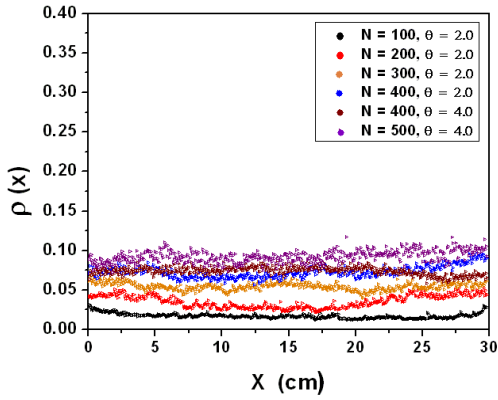


Figure 4.10: Density distribution of particles from simulation transverse to the direction of vibration

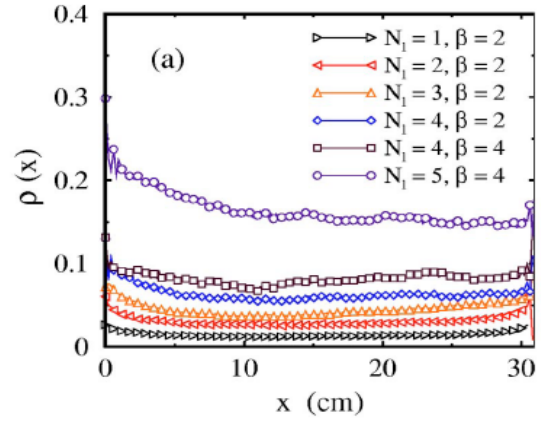


Figure 4.11: Density distribution of particles from experiment transverse to the direction of vibration

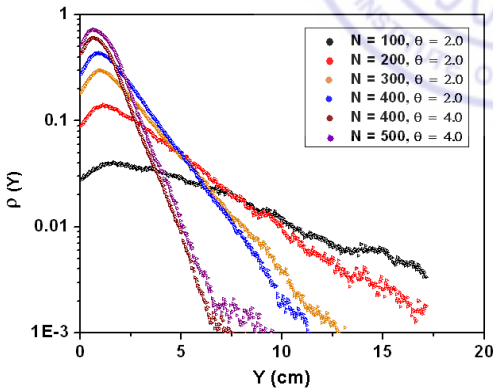


Figure 4.12: Density distribution of particles from simulation along the direction of vibration

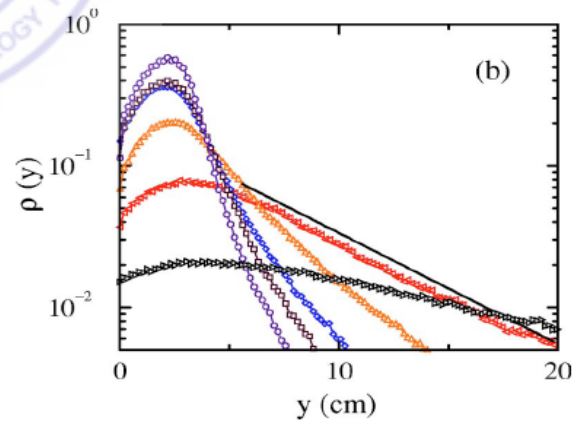


Figure 4.13: Density distribution of particles from experiment along the direction of vibration

Chapter 5

Results and discussion

In this chapter, various results for mono-disperse granular system are discussed. We explore the effect of the vibration amplitude A , taper ϕ , the inclination angle θ , and the area fraction η on the flow rates of particles from top and bottom ends of vibrating channel at various vibration frequencies ν . We do not study the effect of friction and damping on the flow rates. In the sections below, all results are non-dimensionalized with acceleration due to gravity g , and the diameter and mass of the grains. As described before, one unit of simulation time equals 0.018 s. Channel's geometrical parameters, i.e., upper width (U), lower width (L), and transverse width (H) are shown in Fig. 5.1. In our results, we plot how the fractional flow rate varies with the vibration frequency by fixing all but a few of the remaining parameters. The fractional flow rate in the upward R_f^{up} and downward R_f^{down} direction is defined as the ratio of the number of particles that escape from the system from the top and bottom exit, respectively, per unit time to the total number of particles in the system, i.e.,

$$R_f^{up} = \text{Number of particles escape from system from top}/(N \times t) \quad (5.1)$$

$$\text{and } R_f^{down} = \text{Number of particles escape from system from bottom}/(N \times t) \quad (5.2)$$

where N is the total number of particles in the system, and t is the total time.

The fractional net flow rate R_f^{net} is the difference between the number of particles flowing

upwards and the particles exiting from the bottom per unit time (Eqn. 5.3).

$$R_f^{net} = R_f^{up} - R_f^{down}. \quad (5.3)$$

The area fraction η is the ratio of area occupied by the particles to the total area of the vibrating channel, and is given by

$$\eta = N \pi \sigma^2 \tan(\phi) / (U^2 - L^2), \quad (5.4)$$

where σ is the particle diameter.

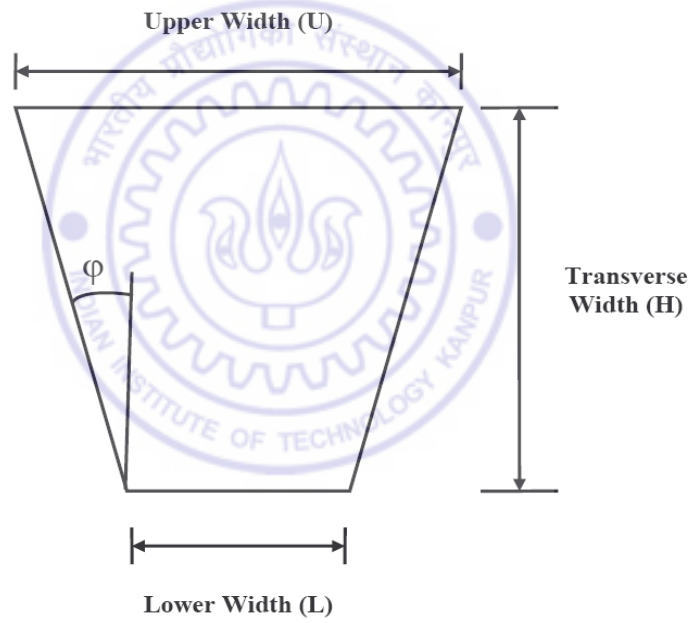


Figure 5.1: Top view of vibrating channel

Finally in all our simulation results, the vibration frequency ν is varied between 1 Hz to 10 Hz.

5.1 Amplitude variation

The channel's vibration amplitude is varied while keeping all other parameters fixed. The simulation parameters for this simulation study are: the amplitude A is varied from 1 particle diameter to 2.5 particle diameter, the number of particles N are 250, the channel's upper U and lower widths L is kept at 30 and 8 particle diameter, respectively, and the channel's inclination θ and taper ϕ are 1° and 30° , respectively.

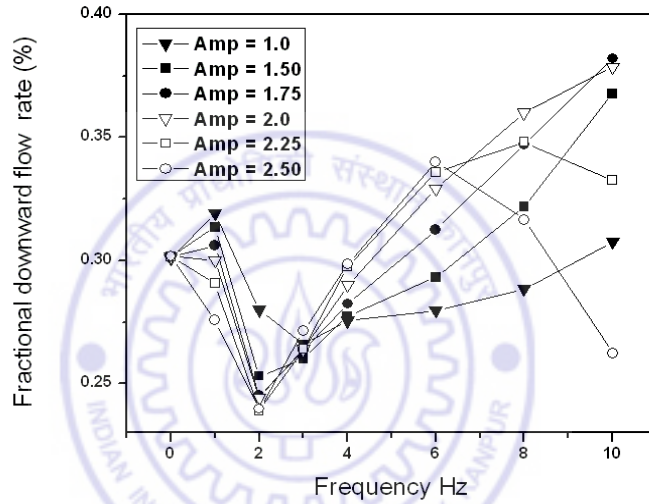


Figure 5.2: Effect of vibration amplitude on the downward flow rate of grains

In Fig. 5.2 we plot downward flow rate R_f^{down} vs. the vibration frequency ν for different amplitudes. It is clear from Fig. 5.2 that the downward flow rate of particles decreases when increasing the frequency up to 2 Hz at higher amplitudes. The reduction in flow rate is due to the particles' collective motion at lower frequencies. Particles move as a solid mass at lower frequencies which increases jamming in the system. Jamming is a solid like state when grains lock themselves and do not move as a single entity. At a vibration amplitude of 1 particle diameter, the flow rate continues to reduce till vibration frequency of 3 Hz, which also indicates the grains' bulk motion. At higher frequencies, the system becomes

fluidized and correspondingly the jamming effect decreases which enhances the downward flow of particles. This bulk behavior may be verified by some auto-correlation tests that should be done. At vibration amplitudes of 2.25 and 2.50 particle diameter, downward flow rate of particles starts decreasing again at higher frequencies.

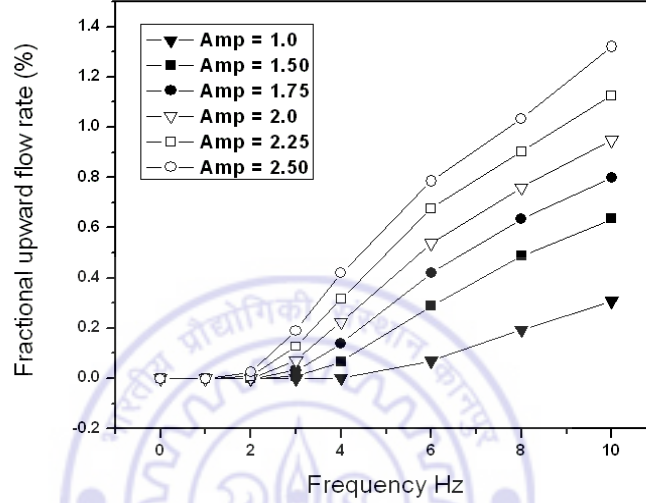


Figure 5.3: Effect of vibration amplitude on the upward flow rate

In Fig. 5.3 we plot upward flow rate R_f^{up} vs. the vibration frequency for different amplitudes. It is observed from Fig. 5.3 that, at low vibration frequencies, there is negligible flow of particles in the upward direction. However, the flow increases with an increase in the frequency at a particular vibration amplitude. At low frequencies, the momentum transfer due to the walls is dominated by the particles' collective motion, which prevents the particles from moving upwards. But, at higher frequencies, the collective motion of grains reduces, and particles easily escape from the system. It is also noticed that at a vibration amplitude of 1, the upward flow rate is almost zero till a frequency of 3 Hz. On the other hand, at amplitudes of 2 and more, the frequency at which particles begin to move upwards lowers to 2 Hz. This also indicates that the upward flow rate is a compromise between the grains' bulk or solid behavior, and the momentum transfer from the channel's walls.

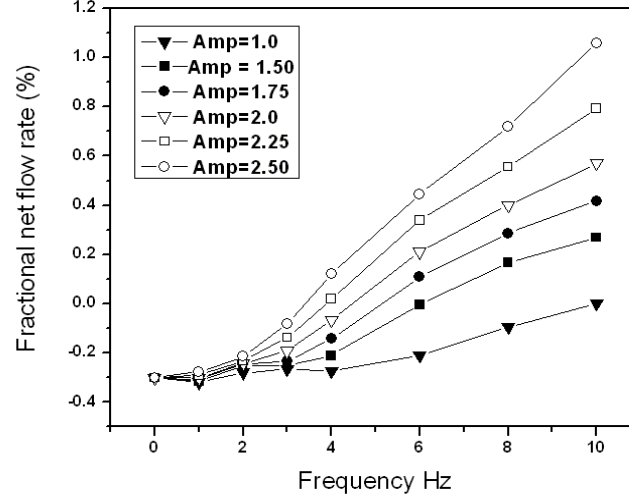


Figure 5.4: Effect of vibration amplitude on the net flow rate.

Figure 5.4 plots the fractional net flow rate R_f^{net} vs. vibration frequency for different amplitudes A . It is observed that the net flow rate of particles increases with the vibration frequency. The frequency at which grains' net flow rate vanishes is the critical frequency at that vibration amplitude. It is also clear from the Fig. 5.4 that the critical frequency decreases with growing amplitude. This makes physical sense, because the rate of upward collisional momentum should increase as $\nu^2 A$.

5.2 Theta variation

The channel's inclination angle is varied to observe the gravity's effect on the flow rate. The simulation parameters for this study are: inclination angle θ is varied from 1° to 2° , the amplitude A is kept fixed at 2 particle diameters, the number of particles N are 250, the channel's upper U and lower widths L are fixed at 30 and 8 particle diameters, respectively, and the channel's taper ϕ is kept fixed at 30° .

Apart from the jamming effect discussed above, it is clear from the graphs of Figs. 5.5 and

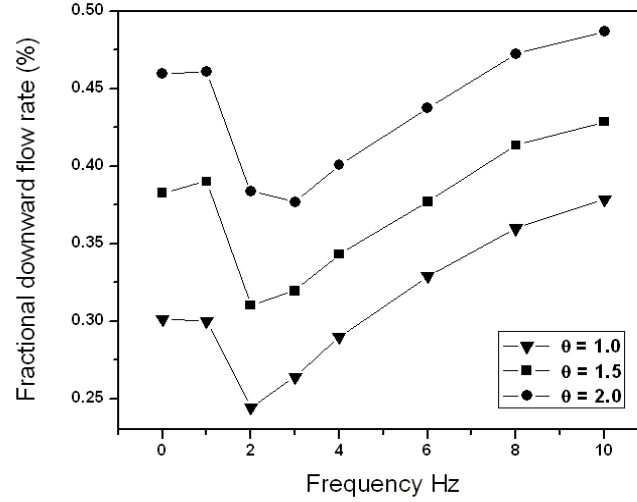


Figure 5.5: Effect of inclination on the grains' downward flow rate.

5.6 that increasing the inclination angle accelerates the particles' downward flow rate, while, correspondingly, decreasing their upward flow rate. This effect is easily explained, because gravity dominates at higher inclination angles, thereby accentuating a grain's tendency to move down.

In Fig. 5.7 we plots the fractional net flow rate vs. vibration frequency for different inclination. It is seen that the net flow rate increases with the frequency, which also suggests the dominant effect of gravity on the flow rates.

5.3 Area fraction variation

The effect of varying the grains' area fraction on their flow is investigated now. The area fraction is varied by changing the number of particles in the system. The simulation parameters are: the amplitude A is kept fixed at 2 particle diameters, the number of particles N are varied from 150 to 250, the channel's upper U and lower widths L are kept 30 and 8 particle diameters, respectively, and the channel's inclination θ and taper ϕ is maintained at

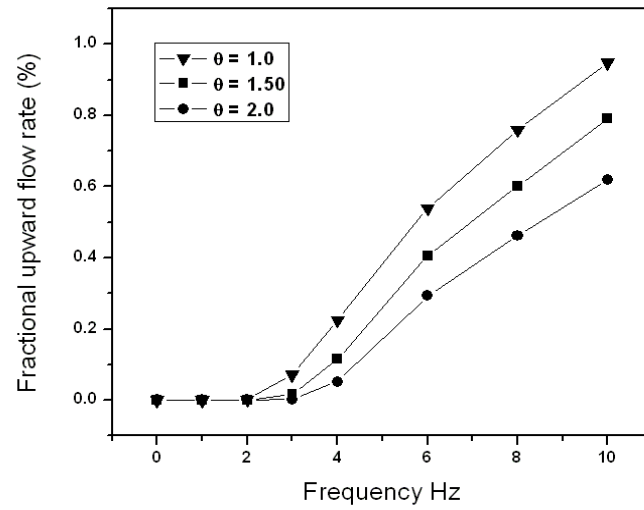


Figure 5.6: Effect of inclination on the upward flow rate.

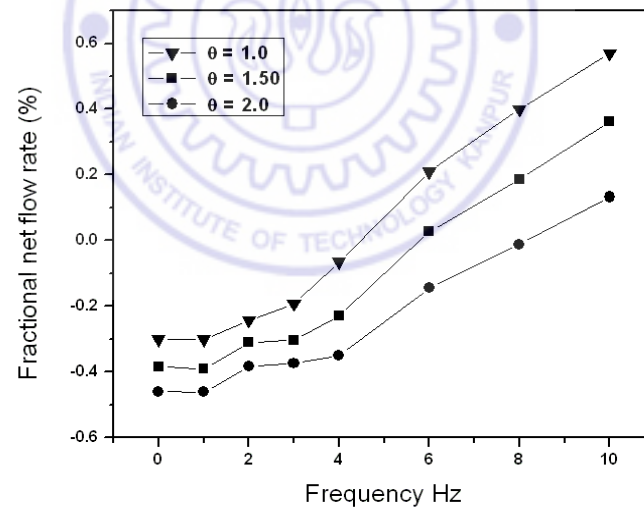


Figure 5.7: Effect of inclination on the net flow rate.

1° and 30° , respectively.

The area fraction η for different number of particles is given in the Tab 5.1.

Table 5.1: Area fraction for different number of particles

Number of particles N	Area fraction η
150	0.325
200	0.434
250	0.542

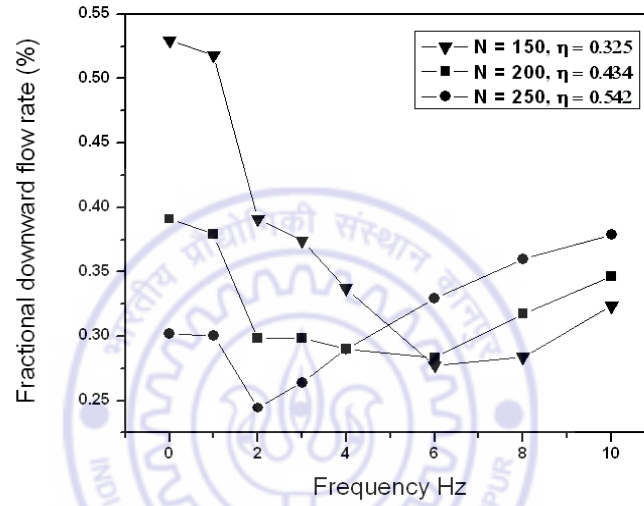


Figure 5.8: Effect of area fraction on the grains' downward flow rate

Figure 5.8 plots the fractional downward flow rate vs. vibration frequency for different number of particles. It is observed that at higher area fractions, the communication between particles increases, which in turn accentuates jamming in the system. At lower area fractions, jamming reduces. Also, as discussed in Sec. 1, the downward flow rate first decreases and then increases with the vibration frequency. This trend is also seen in the graphs of Fig. 5.8. However, the frequency, up to which the downward flow rate decreases, increases at less number of particles.

In Fig. 5.9, grains' fractional upward flow rate is plotted against the vibration frequency for different number of particles. As we observed in previous sections that the particles'

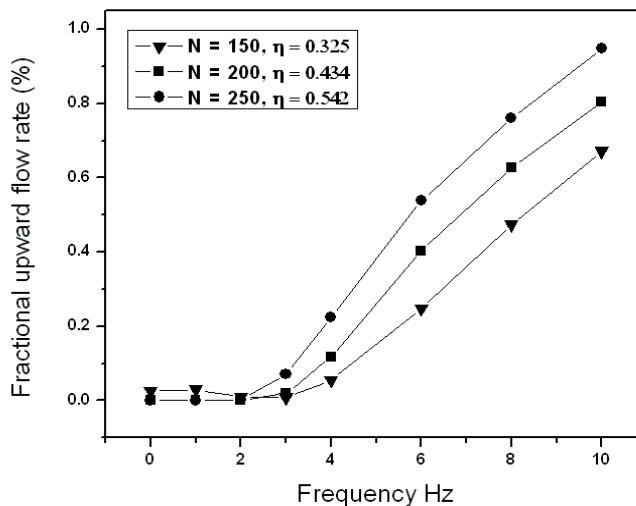


Figure 5.9: Effect of area fraction on the upward flow rate

upward flow rate is zero at low frequencies, and grows with an increase in the vibration frequency (see Figs. 5.3 and 5.6). At an area fraction corresponding to 150 particles, the upward flow rate is not zero as in the case of 200 and 250 particles. This is because of its low area fraction. As the density of the system is low, so is the effective viscosity, i.e., not many particles are present to resist the motion of inserted particles. As a result, even at very low frequencies, even the gentlest of collision with the system's slanted walls causes a particle to escape upwards. To check this phenomenon, we lowered the inserted height, but the results we got were the same.

Figure 5.10 shows the variation of net flow rate with vibration frequency for different number of particles. It is clear that the particles' net flow rate increases with the vibration frequency.

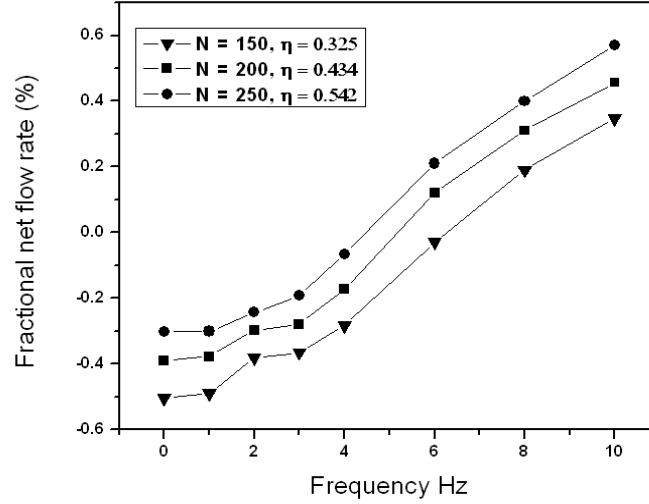


Figure 5.10: Effect of area fraction on the net flow rate

5.4 Variation in the channel's taper

Channel's taper plays an important role in transferring upward momentum to the grains. We have done two simulation studies in which the taper is varied. In the first case, the channel's inclination angle is kept zero, while in the second, the inclination angle is set to 1° .

In both cases, the simulation parameters are: the amplitude A is maintained at 2 particle diameters, the channel's lower width L is set to 8 particle diameter. The channel's upper width is varied with the taper and number of particles to keep the area fraction η and transverse length H same. It is given in Tab. 5.2.

5.4.1 Zero inclination angle

In this case, the vibrating channel is not inclined with the ground. In Fig. 5.11 we plots the particles' fractional downward flow rate vs. the vibration frequency for different taper values. It is observed that at a fixed frequency, increasing the channel's taper decreases

Table 5.2: Upper width of shaking channel for different taper values

No. of Particles	Taper(in degree)	Upper Width
105	0.0	8
168	15.0	18
250	30.0	30
360	45.0	46
540	60.0	74

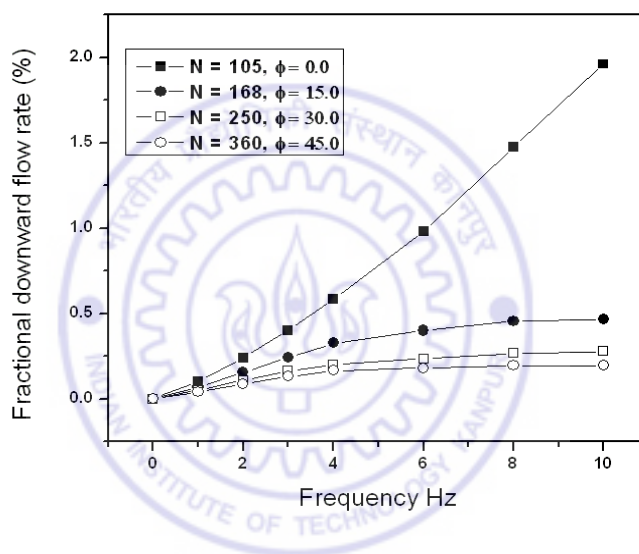


Figure 5.11: Effect of varying the channel's taper on downward flow rate at zero inclination angle.

the particles' downward flow rate. This may be due to the jamming in higher number of particles. It is also clear that the downward flow rate first increases with frequency, and then becomes constant at higher frequencies, except at zero taper, where the downward flow rate of particles increases almost linearly with frequency. The reason for constant downward flow rate at higher frequencies need to be investigated.

Figure 5.12 illustrates the variation in the fractional upward flow rate with the vibration

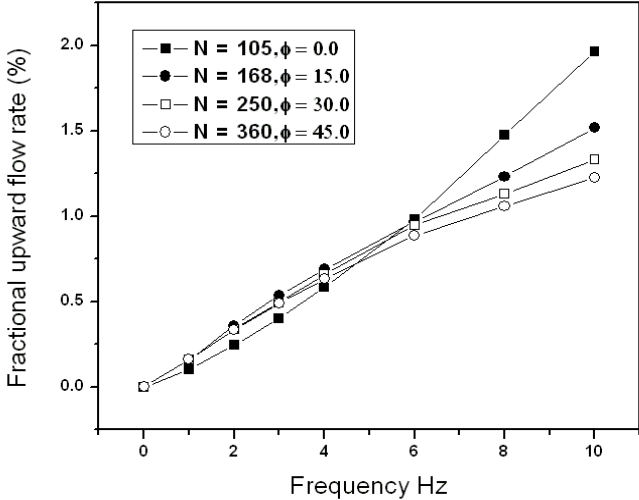


Figure 5.12: Effect of varying the channel’s taper on upward flow rate at zero inclination angle.

frequency. It is clear that the upward flow rate decreases with an increase in the taper at a fixed frequency. This observed phenomena is in reverse of the expected behavior, because increasing the taper angle enhances the upward flow rate. We think that some correlations parameters, i.e., velocity auto-correlation function (VACF), root mean square displacement (RMSD) may give some explanation for this surprising behavior.

In Fig. 5.13 we plots the fractional net flow rate vs. the vibration frequency for different taper values. It is observed that the fractional net flow rate increases with the channel’s taper. At zero taper, the net flow rate is zero, as illustrated in Sec. 4.3 of Chapter 4, but at higher taper angles the net flow rate increases with frequency. At taper angles of 30° and 45° , it is observed that the net flow rate is same in a frequency region of 4 - 9 Hz and three curves corresponding to taper of 15° , 30° and 45° meets at one point corresponding to 10 Hz vibration frequency. This suggests that at higher frequencies, the channel’s taper doesn’t effect the net flow rate much.

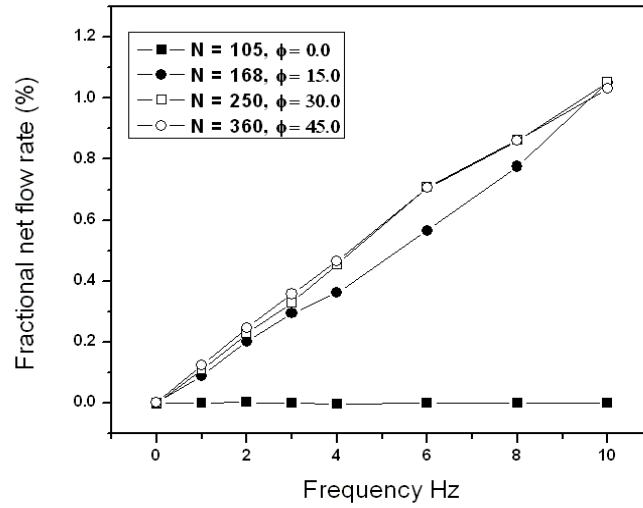


Figure 5.13: Effect of varying the channel's taper on net flow rate at zero inclination angle

5.4.2 1° inclination angle

We now incline the channel at 1° to the ground.

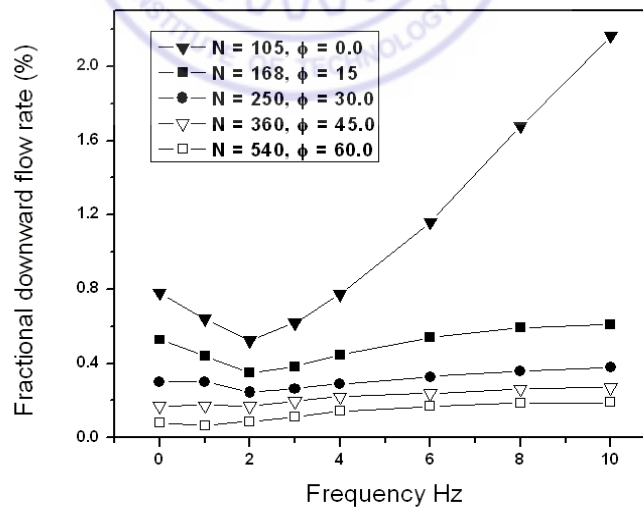


Figure 5.14: Effect of the taper on the downward flow rate in a channel inclined at 1° .

Figure 5.14 shows the variation of the fractional downward flow rate with the vibration frequency. It is seen that the variation in downward flow rate is similar to the case of zero inclination. However, the upward flow rate (see Fig. 5.15) the flow rate decreases

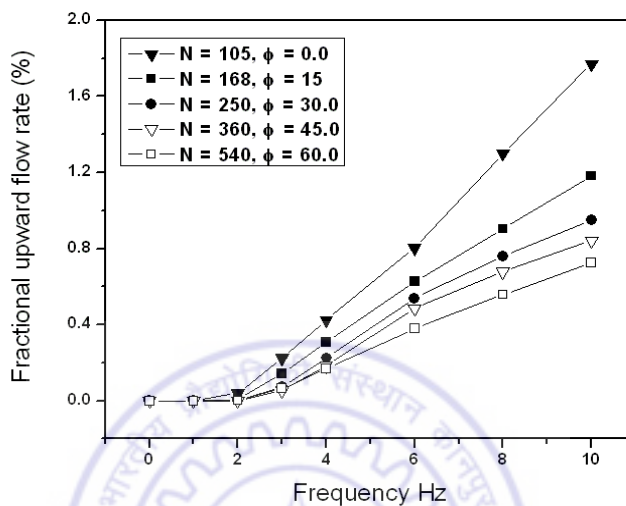


Figure 5.15: Effect of the taper on the upward flow rate in a channel inclined at 1° .

with increasing taper at a fixed frequency. The curve corresponding to zero taper does not intersect other curves as it did when there was no inclination; cf., Fig. 5.12.

Figure 5.16 illustrates the variation in the fractional net flow rate with the vibration frequency for different channel's taper. It is clear that at zero taper, the net flow rate increases with frequency up to 4 Hz, beyond which it starts decreasing. This shows that at higher frequencies, the downward flow dominates upward flow. However, in other cases, except when the taper equals 60° , the net flow rate increases with the vibration frequency. At a 60° taper, the net flow rate is less compared to flow rates at taper values of 30° and 45° beyond a frequency of 5 Hz.

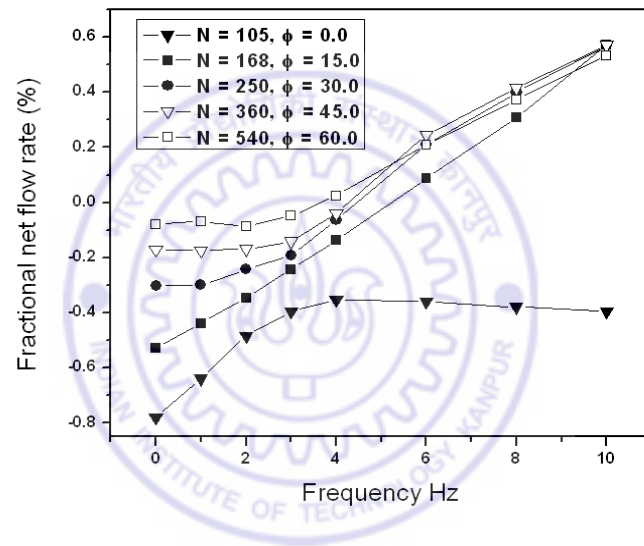


Figure 5.16: Effect of the taper on the net flow rate in a channel inclined at 1° .

Chapter 6

Conclusions

6.1 Conclusion

In this work, we focused on the effect of various parameters, i.e., the vibration amplitude A , frequency ν , inclination (θ), taper (ϕ) and area fraction (η) on the flow rate of mono-disperse grains vibrated in a slightly inclined and tapered channel displayed in Fig. 1.1. We identified the presence of a critical frequency at which the flow of these grains reverses. This critical frequency is seen to depend on the grains' physical characteristics such as inter-particle friction, its diameter and density etc. We believe that this difference in the critical frequency for various species may be the mechanism that produces segregation in binary mixtures, i.e., if the system is shaken at a frequency at which grains of one kind preferentially move downwards, segregation may occur. This, of course, is to be tested, and simulations to this end are being undertaken. We observed that the dynamics of the system is very sensitive to inclination, indicating the need for its proper control.

We also investigated the effect of the area fraction on the particles' flow rates and it is observed that jamming reduces at low area fractions. Effect of the channel's taper on the particles' flow rates is also observed, and the anomalous reduction of the upward flow rate at higher taper angles was noted.

6.2 Future work

In the present study, we concentrated our efforts on the dynamics of mono-disperse granular particles. To gain more confidence in present simulation results, there is a need to conduct an experimental study of mono-disperse granular system. Following work has to be done in order to gain more understanding of the current segregation phenomenon.

1. Investigation of effect of particle diameter, and its density on the critical frequency
2. Effect of inter-particle friction on the flow rates .
3. Variation in flow rates of particles with friction between particle and channel's surface and side walls.
4. Critical vibration frequency at different vibration amplitude in shifted Christmas tree type geometry of shaking channel in mono-disperse granular system.
5. Finally, we intend to simulate the dynamics of binary systems first in the trapezoidal geometry of Fig. 1.2, and then in the more intricate shape displayed in Fig. 1.1. This will test our earlier hypothesis regarding the geometry being simply a concatenation of micro-sorting chambers

Bibliography

- Allen, M. P. and Tildesley, D. J. (1987). *Computer Simulation of Liquids*. Oxford Science Publications, New York.
- Asmar, B., Langston, P., Matchett, A., and Walters, J. (2002). Validation tests on a distinct element model of vibrating cohesive particle systems. *Computers and Chemical Engineering*, 26:785–802.
- Blair, D. L. and Kudrolli, A. (2003). Collision statistics of driven granular materials. *Phys. Rev. E*, 67:041301.
- Brilliantov, N. V., Spahn, F., Hertzsch, J. M., and Poschel, T. (1996). A model for collision in granular gases. *Phys. Rev. E*, 53:5382.
- Cundall, P. A. and Strack, O. D. L. (1979). A discrete numerical model for granular assemblies. *Geotechniques*, 29:47.
- Frenkel, D. and Smit, B. (1996). *Understanding Molecular Simulation: From Algorithms to Applications*. Academic Press, San Diego.
- Hong, D. C. and Quinn, P. V. (2001). Reverse brazil nut problem: Competition between percolation and condensation. *Phys. Rev. Lett.*, 86:3423–3426.
- Jaeger, H. M. and Nagel, S. R. (1996). Granular solids, liquids, and gases. *Rev. Mod. Phys.*, 68:1259–1273.
- Johnson, K. L. (1985). *Contact Mechanics*. Cambridge University Press, Cambridge.
- Knight, J. B., Jaeger, H. M., , and Nagel, S. R. (1993). Vibration-induced size separation in granular media: The convection connection. *Phys. Rev. Lett.*, 70:3728–3731.
- Kudrolli, A. (2004). Size separation in vibrated granular matter. *Reports on Progress in*

- Physics*, 67:209–247.
- Levanon, M. and Rapaport, D. (2001). Stratified horizontal flow in vertically vibrated granular layers. *Phys. Rev. E*, 64:011304.
- Medved, M., Dawson, D., Jaeger, H. M., and Nagel, S. R. (1999). Convection in horizontally vibrated granular material. *CHAOS*, 93:691–696.
- Mishra, B. K. (2003). A review of computer simulation of tumbling mills by the discrete element method: Part 1-contact mechanics. *Int. J. Miner. Process.*, 71:73–93.
- Mobius, M. E., Lauderdale, B. E., Nagel, S. R., and Jaeger, H. M. (2001). Size separation of granular particles. *Nature*, 414:270.
- Poschel, T. and Schwager, T. (2005). *Computational Granular Dynamics: Models and Algorithms*. Springer, Berlin.
- Rapaport, D. (2002). Simulational studies of axial granular segregation in a rotating cylinder. *Phys. Rev. E*, 65:061306.
- Rapaport, D. (2007). Radial and axial segregation of granular matter in a rotating cylinder: A simulation study. *Phys. Rev. E*, 75:031301.
- Rapaport, D. C. (2004). *The Art of Molecular Dynamics Simulation*. Cambridge University Press, Cambridge.
- Ristow, G. H. (1994). Granular dynamics: A review about recent molecular dynamics simulations of granular materials. *Ann. Rev. of Comp. Phys.*, 1:275–308.
- Rosato, A., Strandburg, K. J., Prinz, F., and Swendsen, R. H. (1987). Why the Brazil nuts are on the top: Size segregation of particulate matter by shaking. *Phys. Rev. Lett.*, 58:1038–1040.
- Sanders, D. A., Swift, M. R., Bowley, R. M., and King, P. J. (2004). Are Brazil nuts attractive? *Phys. Rev. Lett.*, 93:3423–3426.
- Schnautz, T., Brito, R., Kruelle, C. A., and Rehberg, I. (2005). A horizontal brazil-nut effect and its reverse. *Phys. Rev. Lett.*, 95:028001.
- Shinbrot, T. and Muzzio, F. J. (1998). Reverse buoyancy in shaken granular beds. *Phys. Rev. Lett.*, 81:4365–4368.